Received: 1 August 2025 | Revised: 2 February 2026 | Accepted: 6 February 2026

DOI: 10.1111/bph.70394

RESEARCH ARTICLE

Second-generation prokineticin PKR_1 receptor agonists: Advancing cardioprotection against chemotherapy-induced toxicity

Anais Audebrand[1] | Simone Brogi[2,3] | Mustafa Tezeren[1,4] | Andrea Tafi[3] | Omer H. Ocak[4] | Hasan Koyuncu[4] | Igor Tetko[5] | Laurent Désaubry[1] | Canan G. Nebigil[1]

[1]INSERM, Regenerative Nanomedicine Laboratory (UMR1260), Faculty of Medicine, FMTS, University of Strasbourg, Strasbourg, France

[2]Department of Pharmacy, University of Pisa, Pisa, Italy

[3]Department of Biotechnology, Chemistry and Pharmacy, University of Siena, Siena, Italy

[4]Ulkar Kimya, G.O.P. Mah, Tekirdağ, Turkey

[5]Institute of Structural Biology, Helmholtz Zentrum München – Research Center for Environmental Health, Neuherberg, Germany

Correspondence
Laurent Désaubry and Canan G. Nebigil, University of Strasbourg, INSERM, Regenerative Nanomedicine Laboratory, Faculty of Medicine, FMTS, Strasbourg, France.
Email: desaubry@unistra.fr; nebigil@unistra.fr

Funding information
European Research Area Network on Cardiovascular Diseases; Fondation de France; Agence Nationale de la Recherche, Grant/Award Number: ANR0005

Abstract

Background and purpose: Anthracycline-induced cardiotoxicity, particularly from doxorubicin, remains a major limitation in cancer therapy, contributing to heart failure and long-term morbidity. Prokineticin receptor-1 (PKR_1), involved in cardiomyocyte survival and anti-fibrotic signalling, represents a promising therapeutic target. This study evaluated the cardioprotective potential of IS39, a novel non-peptide PKR_1 agonist, in models of doxorubicin-induced cardiac injury.

Experimental approach: In silico ADME–toxicity profiling, scaffold optimisation and molecular docking were used to refine non-peptide PKR_1 agonists, replacing the dehydroamide moiety of first-generation compounds with a D-aminoacyl group to enhance metabolic stability. The lead compound IS39 was evaluated *in vitro* in primary cardiomyocytes and *in vivo* in a murine model of doxorubicin-induced cardiotoxicity. Parallel studies assessed potential interference with doxorubicin antitumour activity in breast cancer cell lines and 3D tumour spheroids. Endpoints included cardiomyocyte viability, oxidative stress, fibrotic markers, cardiac function, histopathology and systemic tolerability.

Key results: IS39 selectively activated PKR_1, reduced reactive oxygen species, suppressed profibrotic gene expression and protected cardiomyocytes from doxorubicin-induced cytotoxicity in vitro. These effects were abolished by PKR_1 knockdown or antagonism, confirming on-target activity, and IS39 did not impair doxorubicin antitumour efficacy. In vivo, IS39 preserved left ventricular ejection fraction, attenuated myocardial fibrosis and apoptosis, and improved cardiac morphology. However, systemic IS39 administration exacerbated doxorubicin-associated weight loss and did not improve overall survival.

Abbreviations: CO, Cardiac output; Col1A1, Collagen 1A1; DAPI, 4′,6-Diamidino-2-Phenylindole; DCFDA, 5(6)-Carboxy-2′,7′-dichlorofluorescein diacetate; DOX, Doxorubicin; EC, Endothelial Cell; EGFP, enhanced green fluorescent protein; GAPDH, Glyceraldehyde-3-phosphate dehydrogenase; GFP, Green Fluorescent Protein; GPCR, G Protein-Coupled Receptor; H2A.X, Histone H2A.X; H9c2, Cell Line Derived From Embryonic Rat Cardioblasts; OCHEM, Online Chemical Database and Modelling Environment; PI3K, Phosphoinositide 3-kinase; PK2, Prokineticin-2; TUNEL, Terminal Deoxynucleotidyl Transferase dUTP Nick-End Labelling.

Conclusions and implications: IS39 confers cardioprotection via PKR1-mediated antioxidant and antifibrotic mechanisms. Despite systemic tolerability limitations, these findings support PKR1 as a therapeutic target and justify development of tissue-selective PKR1 agonists for cardio-oncology applications.

KEYWORDS
chemoresistance, doxorubicin, hypoxia, prokineticin 2, reactive oxygen species

1 | INTRODUCTION

Cardiotoxicity remains a major clinical challenge in oncology and internal medicine, with long-term cardiovascular complications emerging as a significant cause of morbidity and mortality among cancer survivors (Nebigil et al., 2020; Zamorano et al., 2016). Despite decades of research into the pathophysiological mechanisms underlying cardiac injury and the development of cardioprotective drugs, clinically approved cardioprotective therapies remain scarce (Audebrand et al., 2019; Biswal et al., 2025).

Most existing therapies for heart failure, such as **ACE** inhibitors, **β-adrenoceptor** antagonists (beta-blockers) and **mineralocorticoid receptor** antagonists (Maddox et al., 2024), were developed to manage haemodynamic imbalance and neurohormonal activation, rather than to directly prevent or reverse cardiac cellular cardiotoxicity (Armenian et al., 2017; Audebrand et al., 2019; Hsu et al., 2021; Linders et al., 2024). Moreover, cardioprotective agents that target precise molecular pathways implicated in chemotherapy-induced cardiac injury have been limited by suboptimal efficacy in large clinical trials because of poor pharmacokinetics and limited tissue specificity (Cardinale et al., 2015; Lyon et al., 2020).

This therapeutic gap is particularly critical in the context of doxorubicin (DOX)-induced cardiotoxicity (Nebigil & Desaubry, 2018), a dose-limiting adverse effect, affecting approximately 9% of patients within a year of exposure and up to 26% at 10 years, according to long-term cohort studies (Armenian et al., 2017; Linders et al., 2024). There is currently no specific treatment for anthracycline-related heart failure beyond conventional heart failure regimens, underscoring the urgent need for novel agents that can both protect cardiac tissue without diminishing oncological efficacy.

Cardioprotective G protein-coupled receptor (GPCR) signalling provides a promising therapeutic avenue. GPCRs play pivotal roles in regulating cardiomyocyte survival, angiogenesis, anti-apoptotic signalling, and the modulation of inflammatory and fibrotic responses (Wang et al., 2018). Despite this therapeutic potential, selective small-molecule GPCR agonists with favourable pharmacokinetic and safety profiles remain underrepresented in the clinic.

One particularly promising target is the **prokineticin receptor-1 (PKR_1)**, a class A GPCR that promotes cardiomyocyte survival and maturation (Arora et al., 2025; Urayama et al., 2007), inhibits fibrosis, and regulates energy homeostasis (Dormishian et al., 2013; Nguyen et al., 2013; Szatkowski et al., 2013), thereby supporting cardiac repair (Nebigil, 2017; Vincenzi et al., 2023; Vincenzi & Nebigil, 2025). The non-peptide selective PKR_1 agonist, IS20, developed using in silico strategies (Gasser et al., 2015) displayed beneficial effects in preclinical DOX-induced cardiotoxicity models (Gasser et al., 2019), but its dehydroamide scaffold confers metabolic instability, thereby limiting its translational potential.

To address these limitations, IS39, a novel, metabolically stable, tyrosine-based PKR_1 agonist, was designed. In this study, we present pharmacological characterisation and preclinical efficacy of IS39 in cellular and animal models of DOX-induced cardiac injury, demonstrating robust cytoprotective and anti-fibrotic activity via selective PKR_1 activation without altering anti-tumour effects of DOX. Although IS39 enhanced DOX-associated weight loss, which likely contributed to the lack of improvement in overall survival, its favourable cardiac profile identifies PKR_1 agonism as a promising strategy for the development of next-generation cardioprotective agents in oncology and potentially for the treatment of metabolic cardiomyopathy.

What is already known

- Doxorubicin cardiotoxicity severely limits cancer treatment, with no specific cardiac therapy available.
- PKR_1, a cardioprotective GPCR, can be targeted by non-peptide agonists like IS20.

What this study adds

- IS39 is a novel, metabolically stable PKR_1 agonist with improved drug-like properties.
- IS39 protects against doxorubicin-induced cardiac injury without compromising antitumour efficacy.

Clinical significance

- IS39 highlights PKR_1 agonism as a strategy to prevent chemotherapy-induced cardiotoxicity.
- PKR_1 ligand development may enable targeted therapies for cardiovascular and metabolic disorders.

2 | METHODS

2.1 | Materials

2.1.1 | Reagents and cell lines

Rat embryonic cardiomyoblasts (H9c2; CRL-1446), human cardiomyocytes (AC16; CRL-3568), human aortic endothelial cells (HAEC; CRL-4052, RRID:CVCL_Z065), Chinese hamster ovary cells (CCL-61, RRID:CVCL_0214) and the breast cancer cell line, MDA-MB-231 (RRID:CVCL_0062) were obtained from the American Type Culture Collection (ATCC, Rockville, MD, USA). Green fluorescent protein (GFP)-expressing human umbilical vein endothelial cells (ECs) (PELOBiotec Cat# PB-CAP-0001GFP), human pulmonary fibroblasts (FBs, PELOBiotec Cat# PB-CH-450-0811) and the respective growth media were purchased from PELOBiotech GmbH (Planegg, Germany). Cell culture media were purchased from PELObiotech GmbH (Planegg, Germany).

Culture ware included T75 flasks (Corning, NY, USA), clear-bottom black 96-well plates and ultra-low-attachment 96-well plates (ULA; S-Bio, Hudson, NH, USA). Key reagents included a cell viability assay kit and white opaque 96-well plates (Nunc), TRIzol reagent, OCT compound, SuperFrost Plus slides, 4′,6-Diamidino-2-Phenylindole (DAPI), Lipofectamine 2000 (all from Thermo Fisher Scientific, Waltham, MA, USA) and doxorubicin hydrochloride (Sigma-Aldrich/Merck, Darmstadt, Germany). Additional chemicals and reagents such as Triton X-100, bovine serum albumin (BSA), Eukitt, dextran T250, sucrose, $CaCl_2$, Tris-maleate buffer, AMP, Pb $(NO_3)_2$, $MnCl_2$, $(NH_4)_2S$ and dihydrorhodamine-123 (DHR-123) were also obtained from Sigma-Aldrich. The PKR_1 agonist PC25 (30 nM) was synthesised by Laurent Désaubry. Apoptosis and reactive oxygen species (ROS) were assessed using the TUNEL and ROS Detection Kits (Abcam). PKR_1 was down-regulated, using siRNA specific for PKR_1 (Dharmacon, Paris France).

2.1.2 | Computational methods and chemical syntheses

Ligand docking was performed using GOLD 3.0.1 (Cambridge Crystallographic Data Centre, UK) employing a genetic algorithm, as previously described (Gasser et al., 2015). IS36, IS37 and IS39 were synthesised via established multi-step procedures detailed in the Supporting Information.

2.1.3 | In silico toxicological and pharmacokinetic assessment

Toxicological and pharmacokinetic properties of IS20, IS37 and IS39 were predicted using QSAR models implemented in the Online Chemical Database and Modelling Environment (OCHEM) platform (Sosnin et al., 2019). Chemical structures were submitted as SMILES strings and evaluated using Registry of Toxic Effects of Chemical Substances (RTECS)-trained models to predict multiple toxicity endpoints, including acute median lethal dose (LD_{50}) and lowest effective/lethal levels (LEL) across available exposure routes, including intraperitoneal dosing.

Pharmacokinetic descriptors, including systemic half-life, plasma protein binding (expressed as predicted free-plasma fraction) and aqueous solubility, were predicted using validated OCHEM models trained on experimental ADME datasets (Tetko et al., 2001). Default model settings and consensus predictions were used where available. Comparative interpretation focussed on relative differences between compounds to guide medicinal chemistry optimisation rather than absolute quantitative accuracy (Han et al., 2025).

2.1.4 | Angiogenesis assay (in vitro)

HAECs were cultured in endothelial cell growth medium supplemented with 10% FBS, 1% endothelial cell growth supplement and antibiotics (penicillin/streptomycin). Cells were seeded onto 24-well plates pre-coated with Matrigel (BD Biosciences, Le Pont-de-Claix, France, #356231) and treated with test compounds (IS20, IS37, IS39) for 16 h. Tube formation was quantified by microscopy at 24 h, as previously described (Gasser et al., 2015; Guilini et al., 2010).

2.1.5 | Internalisation assay

CHO cells stably expressing PKR_1-GFP were seeded on poly-L-lysine–coated glass coverslips. At ~20% confluence, cells were treated with 30 nM IS39 for 30 min at 37°C. Cells were fixed and mounted in Mowiol for imaging. Internalisation was quantified by confocal microscopy and digital analysis, as described previously (Gasser et al., 2015).

2.1.6 | Assessment of kinase pathway activation by detection of protein phosphorylation using Western blot

Cells or murine heart tissues were lysed in cold radioimmunoprecipitation assay (RIPA) buffer supplemented with protease and phosphatase inhibitors (Thermo Scientific, Illkirch, France). Protein content was quantified using a bicinchoninic acid (BCA) assay (Thermo Scientific). Equal amounts (10–30 µg) were resolved by sodium dodecyl sulphate polyacrylamide gel electrophoresis (SDS–PAGE) and transferred to polyvinylidene fluoride (PVDF) membranes (Thermo Scientific). Membranes were probed with antibody against Phosphorylated-H2A.X (ser 139, Cell Signaling, #9718, 1/1000), phosphorylated-Akt (ser 473, #4058, 1/1000) and total-Akt (Cell Signaling, #9272, 1/1000), Phospho-p44/42 MAPK (Erk1) (Tyr204)/(Erk2) (Tyr187) (D1H6G) Mouse Monoclonal Antibody (Cell Signaling #5726), total p44/42 MAPK (Erk1/2) (137F5) Rabbit Monoclonal Antibody (Cell Signaling #4695), Glyceraldehyde-3-phosphate dehydrogenase (GAPDH) (Santa-Cruz, # sc-32233, 1/1000), and vinculin (Cell Signaling, #4650, 1/5000). Membranes were exposed to peroxidase-conjugated secondary antibodies (Santa Cruz, 1/10000),

TABLE 1 Primary and secondary antibodies.

Antibody	Host	Dilution	Source	(RRID) and Cat#/
p-Akt (473) (WB)	Rabbit	1:1000	Cell Signaling Technology	(AB_2315049) #4060
t-Akt (WB)				(C67E7) #4691
Phospho-p44/42 MAPK (Thr202/Tyr204) (WB)	Rabbit	1:1000	Cell Signaling	#9101
total p44/42 MAPK (Erk1/2) (WB)	Rabbit	1/1000		(137F5) #4695
Gamma-H2A.X (Ser139) (WB)	Rabbit	1:1000	Sigma-Aldrich	(clone JBW301) #05-636
GADPH (WB)	Rabbit	1:1000	Sigma-Aldrich	G9545
Vinculin (WB)	Rabbit	1/500		V4139-200UL
Anti-Rabbit IgG (H + L) highly cross-adsorbed secondary antibody, HRP	Goat anti rabbit	1:5000	Thermo Fisher	G-21234
Collogen I and III (Nauck et al.)	Rabbit	1:200	Abcam,	Abcam, #ab34710
MHC (MF20)-I (Nauck et al.)	Monoclonal	1:200	Developmental Studies Hybridoma Bank, University of Iowa	(AB_2147781) #MF20
Goat Anti-Rabbit IgG Alexa Fluor 488 (Nauck et al.)	Goat	1:500	Thermo Fisher	#A-11008
Goat Anti-Rabbit IgG Alexa Fluor 647 (Nauck et al.)		1:500		# A-11001
Goat anti mouse Alexa Fluor™ 488 (Nauck et al.)		1:1000		#A21247

and immunoreactivity was detected with an enhanced chemiluminescence (ECL) Prime chemoluminescence detection kit (Amersham Pharmacia). Signals were detected with ECL Prime (GE Healthcare) chemiluminescence, and band intensities were quantified by densitometry using ImageJ software as previously described (Qureshi et al., 2018). Phosphorylation levels were expressed as the ratio of phosphorylated protein to total protein and normalised to vinculin and control conditions. All the antibodies are listed in Table 1.

2.1.7 | Viability assay and reactive oxygen species (ROS) accumulation in 2D cells

Appropriate 10,000 cells per well H9c2 or AC16 cardiomyocytes and 20,000 MDA-MB 231 breast cancer cells were seeded at 10,000 cells per well in 96-well plates and allowed to adhere for 24 h. Cells were pre-treated with IS39 or IS37 overnight in 1% serum medium before exposure to DOX (10 nM–10 μM) for 24 h. In selected experiments, cells were pre-incubated with the PKR_1 antagonist PC25 (30 nM). Viability was assessed using the CyQUANT-NF Kit (Invitrogen/Thermo Fisher, #C35006), with absorbance measured at 480/520 nm (Gasser et al., 2019).

Intracellular ROS (Biswal et al.) generation in H9c2 cells was assessed using the 2′,7′-dichlorodihydrofluorescein diacetate (DCFDA) ROS Detection Assay Kit (Abcam, Cambridge, United Kingdom, #ab113851) according to the manufacturer's protocol. Following pre-treatment with IS37 and IS39, the cells were washed and incubated with 25 μM DCFDA for 45 min at 37°C in the dark to enable dye loading and de-esterification. Subsequently, the cells were exposed to 15 μM doxorubicin (DOX) for 3 h to induce ROS production. The fluorescence intensity was measured at excitation/emission wavelengths of 485/535 nm using a Fluoskan Ascent Fluorescan Reader (Thermo Scientific) (Gasser et al., 2019).

2.1.8 | Real-time quantitative polymerase chain reaction (PCR)

Total RNA from H9c2 cells or mouse hearts was isolated using TRIzol reagent according to the manufacturer's instructions (Thermo Fisher). RNA concentration and purity were assessed with a NanoDrop spectrophotometer. First-strand cDNA was synthesised from 1 μg total RNA and used as a template for SYBR Green–based qPCR on a MyiQ cycler (Bio-Rad). GAPDH and β-actin were used as endogenous housekeeping controls. All reactions were run in technical triplicates. Relative gene expression was calculated by the $2^{-}\Delta\Delta Ct$ method, normalising target gene Ct values to the geometric mean of GAPDH and β-actin and expressing fold change relative to the control (vehicle-treated) group. Primer sequences for target genes are listed in Table 2.

2.1.9 | Down-regulation of PKR_1

Small interfering RNA-targeting prokineticin receptor-1 (siRNA-PKR_1, siGenome Smart pool cat# M-005593-00; Dharmacon, Lafayette, CO, USA) was employed to silence PKR_1 expression, as previously described (Qureshi et al., 2018). Briefly, human AC16 cardiomyocytes were plated on gelatine-coated dishes and transfected with 100-nM siRNA-PKR_1 using Lipofectamine 2000 (Thermo Fisher, # 11668019) in Opti-MEM medium (Thermo Fisher, # 31985062) for 6 h, followed by replacement with complete culture medium. A scrambled siRNA sequence with no known target in the mouse genome was used as a

TABLE 2 Primers for qRT-PCR.

Gene	Forward	Reverse
Col1A1	5′-TGCTGTCCCTGTATGCCTCTG-3′	5′-TGATGTCACGCACGATTTCC-3′
BNP	5′-AAGTCCTAGCCAGTCTCCAGA-3′	5′-GAGCTGTCTCTGGGCCATTTC-3′
alpha-MHC	5′-GAGATTTCTCCAACCCAG-3′	5′-TCTGACTTTCGGAGGTACT-3′
beta-MHC	5′-CTACAGGCCTGGGCTTACCT-3′	5′-TCTCCTTCTCAGACTTCCGC-3′
β-actin	5′-GAGACCTTCAACACCCC-3′	5′-GTGGTGGTGAAGCTGTAGCC-3′
Mouse *pkr1*	5′-GCTCTGGTTCGCAGGTTGAA-3′	5′-GCAAGGTTGACGACTCCTCT-3′
Mouse *Gapdh*	5′-AGGTCGGTGTGAACGGATTTG-3′	5′-TGTAGACCATGTAGTTGAGGTCA-3′
Fbxo32 (Atg-1)	5′-ATGCACACTGGTGCAGAGAG-3′	5′-TGTAAGCACACAGGCAGGTC-3′
Human *BCL2*	5′-GGAGGATTGTGGCCTTCTTT-3′	5′-GCCCAATACGACCAAATCCGTTGA-3′
Human *BAX*:	5′-CGGAGGCTGGGATGCCTTTG-3′	5′-TCCAATGTCCAGCCTTTG-3′
Human *PKR1*	5′-GCTCTGGTTCGCAGGTTGAA-3′	5′-GCAGTTTCTTGTAGCGGACCA-3′
Human *GAPDH* 5′-	5′-GAAATCCCATCACCATCT-3′	5′-GACTCCACGACGTACTCA-3′

Abbreviations: Atg-1, Atrogin-1; Fbxo32, F-box protein 32.

control. After 48 h, total RNA were extracted to assess knockdown efficiency by qPCR.

2.1.10 | Mouse models of cardiotoxicity

Animal studies complied with Directive 2010/63/EU and were approved by French and European regulatory bodies (APAFIS#4708). Animal studies are reported in compliance with the ARRIVE guidelines (Percie du Sert et al., 2020) and with the recommendations made by the *British Journal of Pharmacology* (Lilley et al., 2020). Male C57BL/6J mice (10 weeks old; Janvier Labs, Le Genest-Saint-Isle, France) received weekly intraperitoneal injections of DOX (5 mg kg^{-1}) for 7 weeks over a 9-week period, as previously described (Gasser et al., 2019). IS39 (1 mg kg^{-1}) or vehicle (0.1% DMSO) was administered daily. Mice were randomly assigned to treatment groups. All efforts were made to minimise suffering with respect to the regulation concerning genetically manipulation of organisms.

Echocardiography was performed in week 9 using a Vevo 2100 system (VisualSonics, Toronto, ON, Canada) under light anaesthesia (1% isoflurane in O_2, Vetoquinol, Magny-Vernois, France). Operators were blinded to group allocation ($n = 10$ mice per group). All echocardiographic parameters measured was obtained from a long-axis view for two-dimensional guided M-mode imaging by the dedicated imaging platform. After echocardiographic analyses, mice were euthanised, and hearts were excised for cryopreservation or histological analysis. All animal experiments were carried out in accordance with current institutional guidelines for the care and use of experimental animals. At the end of experiments, mice were deeply anaesthetised with isoflurane until loss of reflexes was confirmed. Animals were then humanely killed by exsanguination, resulting in permanent cessation of circulation. Death was confirmed by absence of respiration and cardiac activity prior to rapidly tissue harvesting for downstream analyses.

2.1.11 | Histological analyses

Cryosections (5–10 μm) of murine hearts were stained using Mallory's trichrome method (VWR Chemicals, Strasbourg, France) to assess myocardial fibrosis. Tissue morphology and fibrosis were evaluated under LEICA microscopes (MZ95 and DME) and documented with PROGRes C5 digital imaging. The planimetric cross-sectional area of the heart was measured on standardised histological sections using calibrated image-analysis software. Cardiomyocyte cross-sectional area was analysed individually on stained transverse sections, and their areas via cell borders were quantified using ImageJ with either manual tracing or semi-automated thresholding.

2.1.12 | TUNEL assay

The frozen hearts embedded in OCT compound (Tissue-Tek, Villeneuve-d'Ascq, France) were cryosectioned at 7-μm thickness and were fixed with 3.7% formaldehyde and permeabilised by ethanol/acetic acid 2:1 (v/v) solution in −20°C. Terminal deoxynucleotidyl transferase dUTP nick end labelling (TUNEL, Apoptag fluorescein,

Sigma Aldrich/Merck) assays were performed, using an In Situ Cell Death Detection Kit (Sigma Aldrich/Merck, #S7110), according to the manufacturer's instructions (Gasser et al., 2019). The sample was incubated in enzymatic solution for 1 h at 37°C. During this, the terminal deoxynucleotidyltransferase catalyses the addition of dUTP-associated digoxygenin on 3′OH free of DNA strand damage. Anti-digoxygenin antibody conjugated-fluorescein labelled the apoptosis positive cells in green; DAPI stained all nuclei cells in blue. Cells numbers were calculated for TUNEL-positive nuclei among total DAPI-stained nuclei in 10 randomly selected high-power microscopic fields (40X) from 10 section per heart ($n = 5$) for each experimental group, using a fluorescence microscope.

2.1.13 | Immunostaining assay

The heart sections were fixed with 3.7% formaldehyde for 10 min; blocked with a solution containing 10% goat serum, 1% BSA, and 0.1% Tween-20; and then incubated overnight at 4°C with primary antibodies against Col1A1 (Abcam, #ab34710; 1:200), MHC (MF20, Developmental Studies Hybridoma Bank, University of Iowa; 1:200) and PKR_1 (monoclonal antibody raised at the Institut de Génétique et de Biologie Moléculaire et Cellulaire, Illkirch, France). On the following day, antibody binding was detected by incubation with fluorescein-conjugated secondary antibodies (1:500 dilution)—Goat Anti-Rabbit IgG Alexa Fluor 488 (Thermo Fisher, #A-11008) and Goat Anti-Rabbit IgG Alexa Fluor 647 (Thermo Fisher, #A21247)—in blocking buffer for 1 h at room temperature. Finally, nuclei were stained with DAPI. Fluorescence was analysed using a Leica fluorescence microscope, and total pixel density was quantified from 10 random microscopic fields per section in 10 sections per heart ($n = 5$ mice) using NIH ImageJ software (Gasser et al., 2019). All the antibodies have been listed in Table 1. The Immuno-related procedures used comply with the recommendations made by the *British Journal of Pharmacology* (Alexander et al., 2018).

2.1.14 | Breast cancer spheroid (3D) formation and treatments

Human breast cancer spheroids were generated as previously described (Vincenzi et al., 2025). Briefly, the triple-negative breast cancer cell line MDA-MB-231 was maintained in RPMI-1640 medium without Hepes, supplemented with 10% fetal calf serum (FCS) and 40 µg ml^{-1} gentamicin. For spheroid generation, MDA-MB-231 cells, fibroblasts (FB) and endothelial cells (EC) were seeded at a ratio of 1:2:2 in 200 µl per well of spheroid medium in 96-well ultra-low-attachment plates. Spheroid medium was prepared by mixing MDA-MB-231 culture medium with FB and EC growth media in a 1:2:2 ratio (Yakavets et al., 2020; Yu et al., 2021). Plates were incubated at 37°C and 5% CO_2, and spheroid formation and morphology were monitored daily for 7 days using an EVOS XL Core microscope (Thermo Fisher Scientific, Waltham, MA, USA) until mature, compact spheroids were obtained.

For treatment, established breast cancer spheroids were exposed to 10 µM doxorubicin hydrochloride (Dox) for 72 h at 37°C in a humidified incubator with 5% CO_2. In the Dox + IS39 group, 50 nM IS39 was added concurrently with Dox. Control spheroids (Vehicle) and the IS39-alone group received fresh spheroid medium without Dox.

2.1.15 | Viability assay in 3D cancer spheroids

Spheroid viability was assessed using the CellTiter-Glo 3D Cell Viability Assay (Promega, Charbonnières-les-Bains, France) according to the manufacturer's protocol. Briefly, individual spheroids were transferred into white, opaque 96-well plates (Nunc) containing 100 µl of conditioned culture medium per well. An equal volume of CellTiter-Glo 3D reagent was then added to each well; plates were protected from light and shaken for 7 min to promote spheroid lysis, and subsequently incubated at room temperature for 25 min to allow stabilisation of the bioluminescent signal. Luminescence, proportional to ATP content, was recorded using a luminometer (1450 MicroBeta TriLux, PerkinElmer, USA) (Vincenzi et al., 2025). Data have been shown as percent of viability changes.

2.1.16 | Statistical analysis

Data and statistical analysis complied with the recommendations of the *British Journal of Pharmacology* on experimental design and analysis in pharmacology (Curtis et al., 2025). Data are presented as mean ± SEM unless stated otherwise. Data normality was assessed using the Shapiro–Wilk test. Group sizes ($n \geq 5$ biological replicates per condition for statistical comparisons) were determined a priori using G*Power 3.1.9.6 with $\alpha = 0.05$, power = 0.80, anticipated effect sizes derived from Saitoh and Nagase (2018), and estimates of outcome variability. Data are displayed as individual values obtained from three independent experiments for cancer spheroids, each including technical replicates (≥10 spheroids per experiment). Statistical analyses were conducted only when group sizes were ≥5, using independent biological replicates. Comparisons among groups were performed using one-way analysis of variance (ANOVA) followed by Bonferroni's post hoc test for multiple comparisons. A P-value < 0.05 was considered statistically significant. Post-hoc tests were run only if F achieved P<0.05 and there was no significant variance inhomogeneity. All analyses were performed on raw data using GraphPad Prism 8 (GraphPad Software, USA). Significance levels of P < 0.05, 0.01, 0.001 and 0.0001 are denoted by one, two, three and four, symbols (*, **, ***, ****), respectively. Randomisation and blinding were applied throughout in vivo and in vitro experiments.

2.1.17 | Nomenclature of targets and ligands

Key protein targets and ligands in this article are hyperlinked to corresponding entries in the IUPHAR/BPS Guide to PHARMACOLOGY http://www.guidetopharmacology.org and are permanently archived

in the Concise Guide to PHARMACOLOGY 2025/26 (Alexander, Alhosaini et al., 2025; Alexander, Cidlowski et al., 2025; Alexander, Fabbro et al., 2025).

3 | RESULTS

3.1 | In Silico absorption, distribution, metabolism and excretion-toxicity, scaffold optimisation and docking to PKR_1 homology modelling

Our previous modelling studies suggest that the alkene moiety does not form direct contacts with the PKR_1 receptor but only presents the pharmacophoric elements to this receptor in a well-defined geometric orientation. On this basis, the dehydroamino amide of IS20 was redesigned into a tyrosine-derived scaffold (IS37 and IS39; Figure 1a) to enhance drug-like properties while maintaining the productive binding orientation. Toxicological liabilities and pharmacokinetic descriptors of IS20, IS37 and IS39 were predicted in silico using Registry of Toxic Effects of Chemical Substances (RTECS)-trained models implemented in Online Chemical Database and Modelling Environment (OCHEM) across all evaluated endpoints; IS20 exhibited a higher predicted toxicity profile than its analogues, being more toxic than IS37 for every endpoint assessed (including lethal dose 50 [LD_{50}] and lowest effect level [LEL] for intraperitoneal dosing) and more toxic than IS39 in 20 of 29 endpoints.

Despite similar predicted systemic half-lives of approximately 10 h for all three compounds, the tyrosine-based analogues showed marked improvements in both plasma protein binding and aqueous solubility. The predicted free-plasma fraction of IS20 was only 4%, whereas IS37 and IS39 reached 8% and 7%, respectively, indicating a near twofold reduction in protein sequestration. In parallel, IS20 was predicted to be approximately fivefold and 10-old less soluble in aqueous media than IS37 and IS39, respectively. Together, these in silico data suggest that replacement of the dehydroamino amide by a tyrosine-derived scaffold mitigates the poor solubility and high protein binding of IS20, consistent with improved systemic bioavailability and a potentially wider therapeutic window from a medicinal chemistry standpoint.

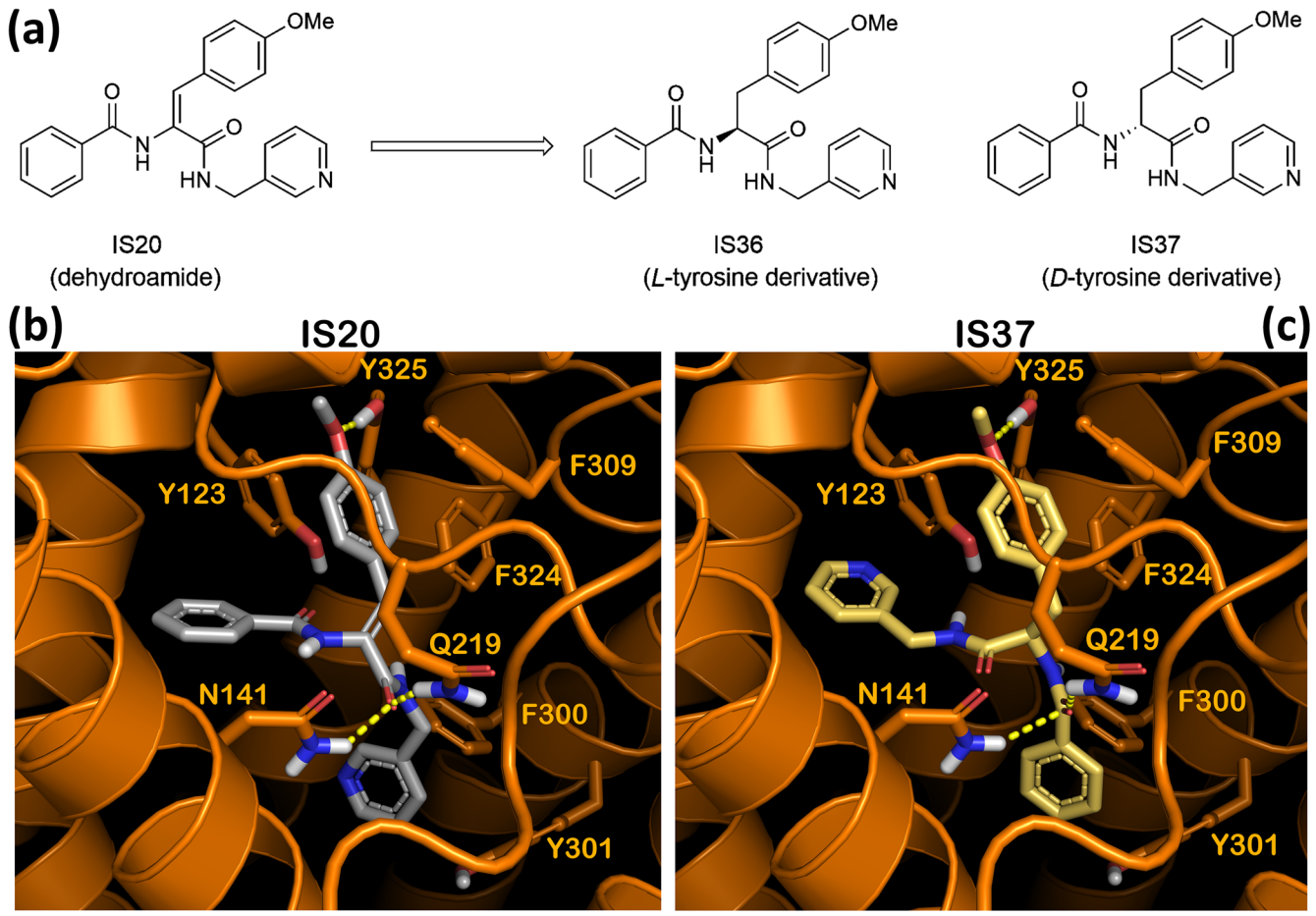

FIGURE 1 **Structure and binding mode of IS20 and IS37 within the PKR_1 binding site. (a)** Chemical structures of IS20 and its dihydro-derivatives IS36 and IS37. **(b,c)** Predicted binding poses of IS20 **(b)** and IS37 **(c)** in the PKR1 homology model (orange cartoon). Ligands binding sites are shown as sticks IS20 (grey) and IS37 (yellow), hydrogen bonds are indicated as yellow dashed lines. The molecular docking analysis highlights key interactions stabilizing IS20 and IS37 with the PKR_1binding pocket.

Docking into the PKR1 homology model revealed that both IS20 and IS37 form key hydrogen bonds (H-bonds) with residues Asn141, Gln219 and Tyr325 and hydrophobic contacts (π-π stacking) with Tyr123 and Phe300 within the orthosteric pocket. IS37 engages additional hydrophobic contacts (π-π stacking) with Tyr301 and Phe309, consistent with the binding mode previously described for IS1 (Gasser et al., 2015). The docking scores (ChemScores) of IS20, IS36 and IS37 were comparable (40.43, 38.21 and 38.90, respectively), supporting that the tyrosine-based analogues retain a binding affinity compatible with PKR_1 agonism (Fig. 1b,c).

3.2 | Chemical synthesis

Tyrosine derivatives were synthesised following the synthetic route disclosed in Scheme 1 (Supporting Information). Boc-O-methyl-D-tyrosine was coupled to 3-picolylamine, deprotected using TFA and acylated to afford derivatives IS37 and IS39. Enantiomer IS36 was obtained similarly using Boc-O-methyl-L-tyrosine.

3.3 | PKR_1 internalisation and ERK activation

We assessed the receptor-binding and activation properties of the novel compounds IS37 and IS39 towards PKR_1 using Chinese Hamster Ovary (CHO) cells stably expressing enhanced green fluorescent protein (EGFP)-tagged human PKR_1 and monitored receptor internalisation, a hallmark of G protein coupled receptor (GPCR) activation. Under basal conditions, confocal microscopy revealed that PKR_1–EGFP was predominantly localised at the plasma membrane (Figure 2a,b, left panels). Upon stimulation with IS37 (30 nM, 30 min) or IS39 (30 nM, 30 min), a pronounced internalisation of PKR_1 was observed, evidenced by redistribution of EGFP fluorescence from the plasma membrane to perinuclear endosomal compartments (Figure 2a,b, right panels). This ligand-induced internalisation demonstrates functional engagement and activation of PKR_1 by both IS37 and IS39. Like IS20, IS37 and IS39 bind to a putative allosteric site of PKR_1 within the transmembrane domain, involving helices II, III, V, VI and VII. This site differs from the orthosteric pocket of the endogenous ligand PK2 (Gasser et al., 2015), precluding the use of a classical radioactive ligand competition assay.

To further support specific ligand–receptor interaction, we examined **MAPK** activation as a functional readout. In CHO cells (which express over 70 endogenous GPCRs), IS37 and IS39 did not increase MAPK activity in cells lacking PKR_1 or expressing PKR_2 (Figure S1A). In contrast, expression of PKR_1 restored MAPK activation by IS39, (Figure S1B), confirming that these ligands act specifically through PKR_1. Furthermore, treatment with IS37 or IS39 elicited a dose-dependent increase in **ERK** phosphorylation in H9c2 cardiomyocytes (Figure 2c,d), consistent with activation of canonical PKR_1

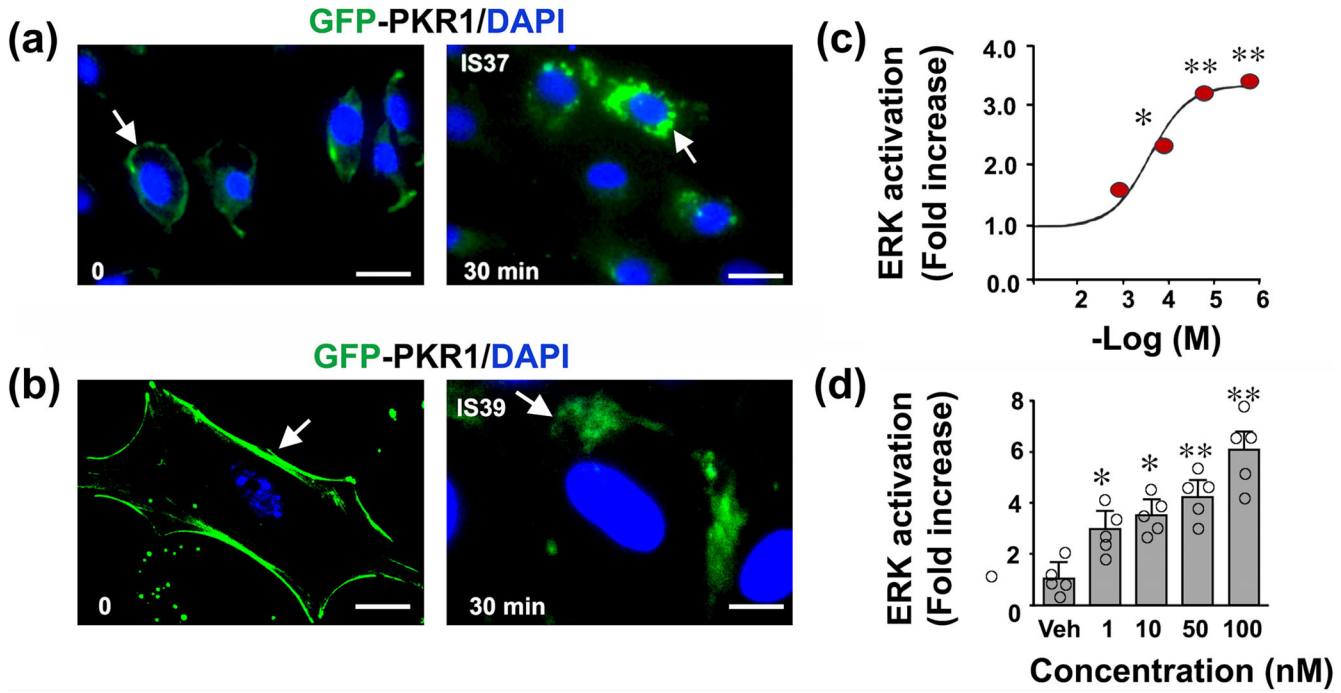

FIGURE 2 **Internalisation of PKR_1 and activation of PKR_1 signalling pathway by IS37 and IS39**. (a, b) Representative confocal images showing the localisation of PKR_1-GFP in CHO cells at baseline (0 min) and 30 min after stimulation with 30 nM IS37 (a) or IS39 (b). Both IS37 and IS39 provoked PKR_1-GFP internalisation within 30 min. Scale bars: 30 μm (a) and 65 μm (b). (c, d) Time- and dose-dependent ERK1/2 activation by IS37 (c) and IS39 (d). Phospho-ERK was quantified by Western blot and expressed as phospho-ERK/total ERK normalised to GAPDH. Data are presented as mean ± SEM from $n = 5$ independent experiments each performed in duplicate. Statistical analysis was performed using one-way ANOVA followed by Bonferroni's multiple comparison test; $^*P < 0.05$ $^{**}P < 0.01$ versus vehicle (DMSO).

downstream signalling pathways implicated in cardioprotection and cell survival (Urayama et al., 2007, 2008).

3.4 | Pro-angiogenic activity of PKR_1 agonists

Given the established role of PKR_1 in promoting endothelial cell function and neovascularisation (Guilini et al., 2010; Urayama et al., 2008), we next evaluated the angiogenic potential of new analogues IS36, IS37 and IS39 using a Matrigel-based tube formation assay (Figure 3). While IS20 served as a reference compound, both IS37 and IS39 demonstrated superior pro-angiogenic activity compared with IS36, suggesting that D-aminoacyl substitution at the scaffold confers improved receptor activation. The comparable potency of IS37 and IS39 suggests that the hydrophobic nature of the acyl moiety may be more critical than its aromaticity in driving PKR_1 agonism. These findings support the structure–activity relationship (SAR) hypothesis that guided the rational design of these analogues.

3.5 | IS39 protects cardiomyocytes from doxorubicin (DOX)-induced cytotoxicity

The cardioprotective potential of IS39 was evaluated in human AC16 cardiomyocytes (Figure 4a) exposed to DOX, a clinically relevant model of chemotherapy-induced cardiotoxicity (Bouleftour et al., 2021). Treatment with DOX (10–1000 nM, 24 h) significantly reduced cell viability in a dose-dependent manner. Pretreatment of AC16 cells with IS39 significantly improved viability in the presence of DOX (Figure 4a). Notably, when PKR_1 expression was reduced by approximately 85 ± 5% via siRNA-mediated knockdown in AC16 cardiomyocytes, the protective effect of IS39 against DOX-induced cytotoxicity was abolished, confirming that the biological activity of IS39 is mediated through PKR_1 (Figure 4b). Similar to IS39, pre-treatment of H9c2 cells with IS37 at concentrations of 10, 30 and 50 nM also significantly attenuated DOX-induced cytotoxicity, particularly at higher DOX concentrations (Figure 4c). Mechanistically, IS39 rapidly activated **Akt** phosphorylation in H9c2 cells, with a maximal response at 30 min after treatment with 30 nM IS39, suggesting engagement of a well-characterised PKR_1–**PI3K**–Akt pro-survival axis (Gasser et al., 2019) (Figure 4d).

3.6 | IS37 and IS39 inhibit doxorubicin (DOX)-induced apoptosis in cardiomyocytes

To further define the anti-apoptotic actions of IS37 and IS39, the activation of H2A.X by phosphorylation as a marker of double-strand DNA break levels was evaluated utilising γ-H2A.X specific antibody (Valceski et al., 2024). Immunoblotting revealed elevated levels of phosphorylated histone variant γ-H2AX following 24 h exposure to 1 μM DOX, reflecting DNA double-strand breaks (Figure 5a). Pre-treatment with IS37 or IS39 reduced γ-H2AX expression by ∼35% (Figure 5b), further substantiating their role in mitigating DOX-induced apoptotic injury.

3.7 | IS39 reduces doxorubicin (DOX)-induced oxidative stress

DOX is known to generate excessive ROS (Biswal et al., 2025), contributing to mitochondrial damage and contractile dysfunction (Nebigil & Desaubry, 2018). Using DCFDA-based fluorescence assays in H9c2 cells, we observed that IS39 (30 nM) reduced DOX (15 μM)-induced ROS accumulation by 23% (Figure 6a), while concomitantly enhancing cell viability by 11% (Figure 6). The cardioprotective effects were abrogated by co-treatment with the PKR_1-specific antagonist PC25 (Figure 6), confirming that the antioxidant and cytoprotective effects of IS39 are mediated through PKR_1 activation.

3.8 | In vivo activation of Akt by IS37 and IS39

To verify the in vivo activity of these PKR_1 agonists, Akt phosphorylation was assessed in cardiac and pulmonary tissue

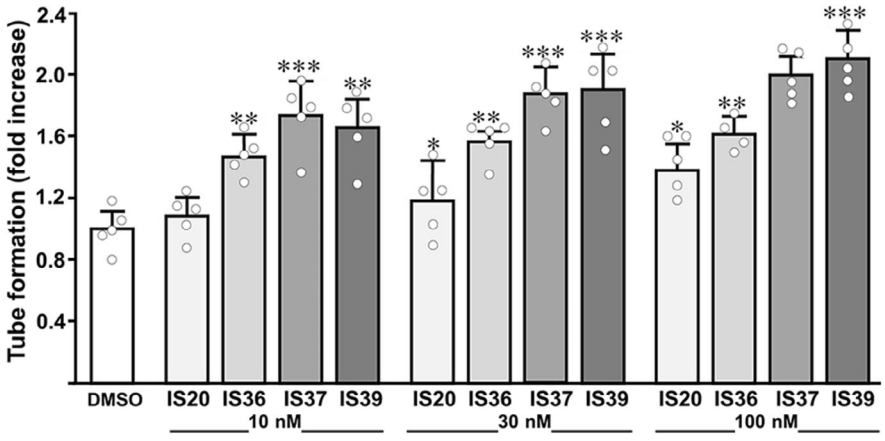

FIGURE 3 **Effect of IS20, IS37, IS39 and analogues on PKR_1-dependent tube formation.** H5V endothelial cells overexpressing human PKR_1 were treated with vehicle (DMSO), IS20, IS37 or IS39 (30 nM), and tube formation (an *in vitro* angiogenesis model) was quantified after 16 h. Data are presented as fold increase versus DMSO, (mean ± SEM from $n = 5$ independent experiments, each performed in triplicate). Statistical analysis was performed using one-way ANOVA followed by Bonferroni's multiple comparison test; $^*P < 0.05$ $^{**}P < 0.01$, $^{***}P < 0.001$ versus vehicle (DMSO) group.

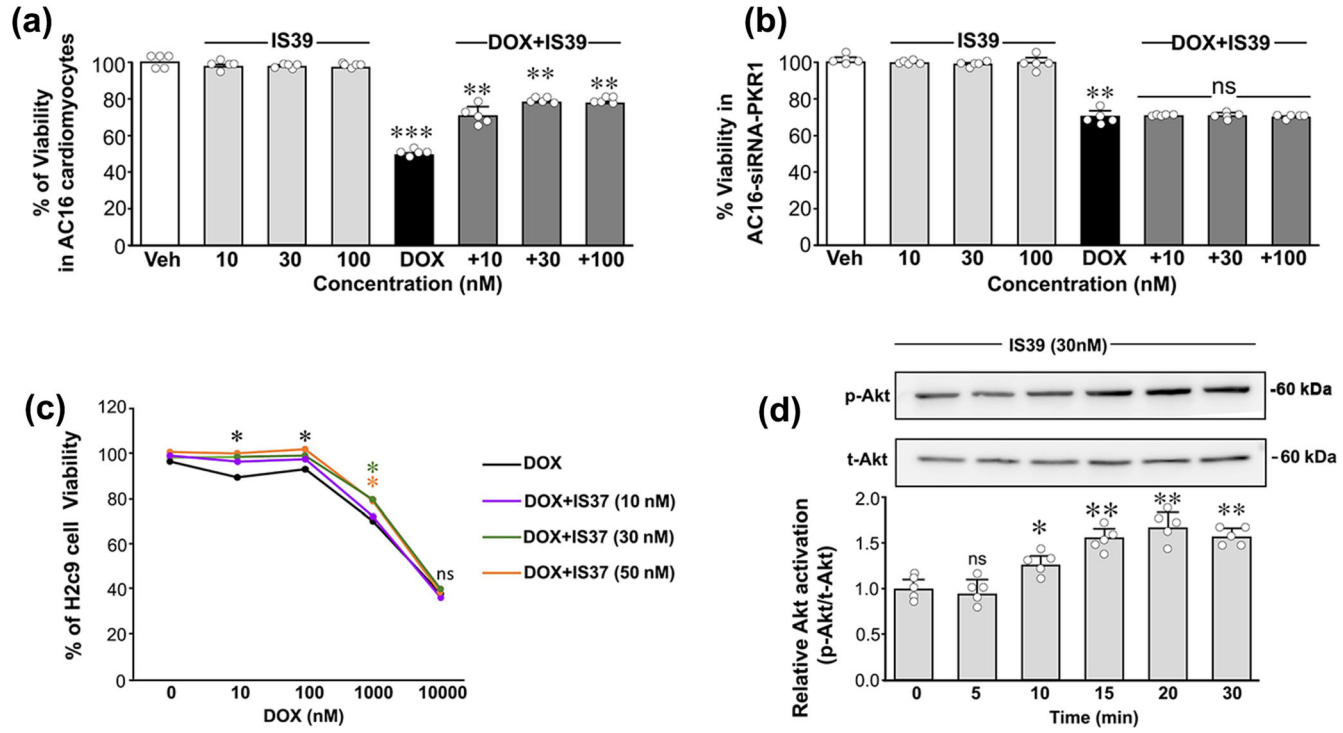

FIGURE 4 **Effect of IS39 and IS37 on doxorubicin (DOX)-induced cytotoxicity and PKR_1 signalling in human AC16 and rat H9c2 cardiomyocytes.** (a) Viability of human AC16 cardiomyocytes exposed to DOX (1 mM), without or with increasing concentration of IS39 (10, 30, 100 nM). (b) Effect of PKR_1 knockdown on viability of AC16 cells transfected with control or PKR_1 siRNA and treated with DOX (1 μM) ± IS39 (10, 30 and 100 nM). Data are mean ± SEM, $n = 5$ independent experiments, each in triplicate. One-way ANOVA followed by Bonferroni's post hoc test: ***P <0.001 versus vehicle (DMSO) group, **P < 0.01 versus DOX group. ns, non-significant versus DOX. (c) Viability of rat H9c2 cardiomyocytes exposed to different concentrations of DOX (nM) in the presence or absence of IS37 (10, 30 and 50 nM). Cell viability was expressed as percent of vehicle (mean ± SEM, $n = 5$ independent experiments, each in triplicate). One-way ANOVA with Bonferroni's test; *P < .05 versus DOX group. (d) Akt activation by IS39 (30 nM) in H9c2 cells. Phospho-Akt levels were quantified by Western blot and expressed as phospho-Akt/total Akt normalised to Vinculin (see Annex), relative to time 0 (mean ± SEM, $n = 5$ independent experiments, each in duplicate). One-way ANOVA with Bonferroni's correction; *P < 0.05, **P < 0.01, ***P < 0.001 versus vehicle.

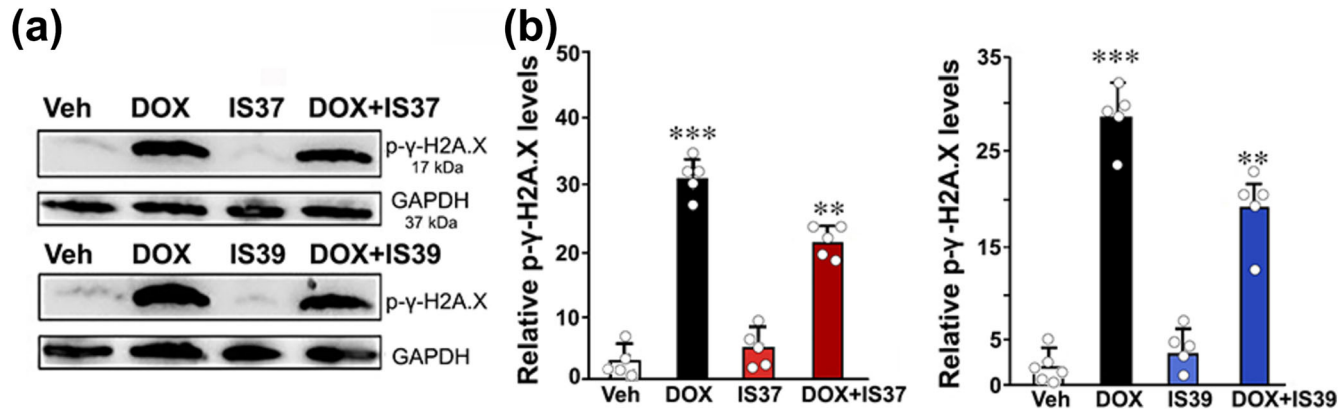

FIGURE 5 **IS37 and IS39 reduce doxorubicin (DOX)-mediated DNA damage.** (a, b) Representative Western blots and densitometric analysis of phospho-γ-H2A.X in H9c2 cells treated with DOX (1 μM) ± IS37 or IS39 (30 nM). Phospho-p-γ H2A.X is expressed as phospho-γ-H2A.X/GAPDH, normalised to vehicle (mean ± SEM, $n = 5$ independent experiments, each in duplicate). Data were analysed by one-way ANOVA with Bonferroni's test; **P < 0.01 vs DOX, ***P < 0.001 versus vehicle.

following intraperitoneal administration of IS37 or IS39 (1 mg kg^{-1}). Ten minutes post-injection, both compounds markedly induced Akt activation in the heart, with 13.2-fold and 9.7-fold increases observed for IS37 and IS39, respectively (Table 3). The effect was less pronounced in lung tissue, indicating some degree of organ selectivity consistent with the cardiac protective aim of these agents.

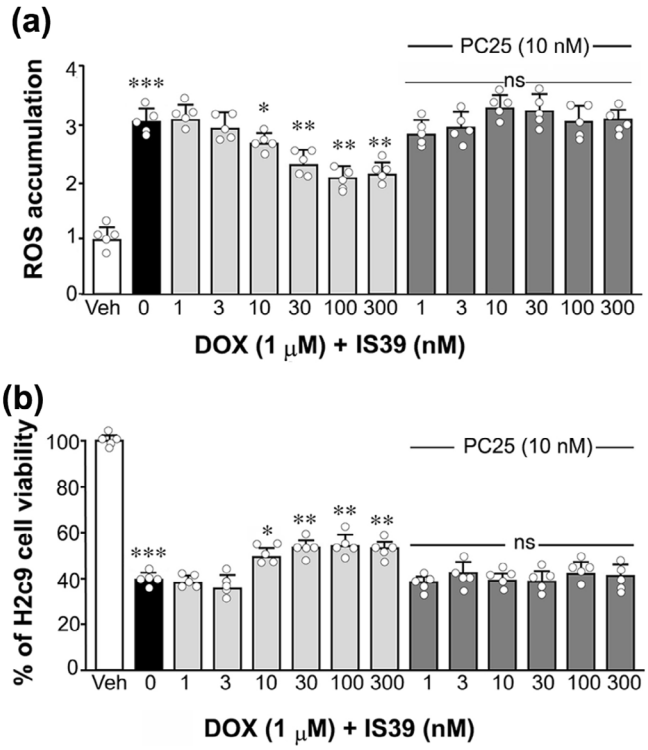

FIGURE 6 **Protective effect IS39 in H9c2 cardiomyocytes against doxorubicin (DOX)-induced oxidative stress and cell death.** (a) Reactive oxygen species (ROS) accumulation in H9c2 cells exposed to DOX (15 μM) ± IS39 (10, 30, 100 nM) with or without the PKR_1 antagonist PC25 (10 nM). ROS are expressed as fold change versus vehicle. (b) Cell viability of H9c2 cells treated in parallel, expressed as percent of vehicle. Data are mean ± SEM from $n = 5$ independent experiments, each performed in triplicate. One-way ANOVA with Bonferroni's multiple comparison test; $^{*}P < 0.05$, $^{**}P < 0.01$ versus DOX, $^{***}P < 0.001$ versus vehicle (DMSO) group. ns, non-significant versus DOX.

TABLE 3 Akt activation in heart and lung 30 min after intraperitoneal injection of IS37 and IS37 into mice ($n = 6$), detected by Western blot analyses of phosphorylated Akt versus total Akt.

Compounds	Heart	Lungs
Vehicle	1 ± 0.2	1 ± 0.2
IS37	13.2 ± 2	3.6 ± 0.5
IS39	9.7 ± 2	4.8 ± 0.8

Note: Data shown as fold increase because of individual variabilities.

3.9 | IS39 mitigates doxorubicin (DOX)-induced fibrosis and apoptosis in a mouse model of chronic toxicity

To evaluate the therapeutic efficacy of IS39 in vivo, a chronic DOX cardiotoxicity mouse model was used, replicating the cumulative anthracycline exposure commonly observed in cancer patients. Mice were administered DOX (5 mg kg^{-1} $week^{-1}$ for 7 weeks) and co-treated with IS39 (1 mg kg^{-1} day^{-1}, i.p.) or vehicle. IS39 significantly attenuated collagen deposition, thereby reducing cardiac fibrosis (Figure 7a,b upper panel and Figure 7c left histogram), and reduced doxorubicin-induced apoptosis in mouse hearts, as shown by TUNEL staining (Figure 7b lower panel and Figure 7c right histogram).

Morphological examination revealed that DOX induced atrophic cardiac remodelling, characterised by reduced heart and cardiomyocyte cross-sectional area with increased fibrosis and apoptosis, while F-box protein 32 (*Fbxo32*) (Atrogin-1 [*Atg-1*]) expression (Figure S2) remained unchanged, indicating that atrophy in this model is better captured by morphometric than by single-gene readouts. IS39 co-treatment largely restored global cardiac dimensions and cardiomyocyte size (Figure 7d,e). Quantitative morphometry showed that the visually larger hearts in the IS39-only group reflected a slight, statistically non-significant increase in heart area, consistent with echocardiographic evidence of a small increase in Left Ventricular End Systolic Diameter (LVESD) without changes in Left Ventricular End Diastolic Diameter (LVEDD), Left Ventricular Ejection Fraction (LVEF), Left Ventricular Fractional Shortening LVFS or cardiac output (CO) (Table 4). Heart-weight-to-body-weight ratios for all groups (Table 5) confirmed the absence of significant cardiac hypertrophy orinducing maladaptive heart growth.

3.10 | IS39 mitigates doxorubicin (DOX)-induced cardiac gene and function alterations in mice heart

RT-qPCR analysis showed that IS39 blunted DOX-induced up-regulation of profibrotic collagen (Col1a1) and hypertrophic markers (e.g. BMP) and attenuated the fetal gene reprogramming from α-MHC to β-MHC in the myocardium (Figure 8a). Consistent with these molecular effects, echocardiography demonstrated a significant improvement in left ventricular systolic function (ejection fraction [EF] %) in DOX + IS39-treated mice compared with DOX alone (Figure 8b and Table 4), indicating attenuation of adverse cardiac remodelling. However, IS39 treatment exacerbated DOX-associated body-weight loss (Figure 8c) and did not improve overall survival (DOX: 54 ± 7% vs DOX + IS39: 51 ± 6%), suggesting that systemic IS39 exposure may induce cachexia-like effects, potentially via hypothalamic or other off-target PKR_1 activation, and underscoring the need for further pharmacodynamic optimisation and/or cardiac-targeted delivery strategies.

3.11 | IS39 did not interfere with doxorubicin (DOX)-mediated anti-cancer efficacy in vitro

To evaluate whether IS39 interferes with the anticancer efficacy of DOX, we first examined its effects in the MDAMB-231 breast cancer cell line. IS39 (10 and 100 nM) did not modify the dose-dependent DOX-induced cytotoxicity (Figure 9a). Consistent with this observation, IS39 did not affect DOX-associated apoptotic markers, including pro-apoptotic BAX and anti-apoptotic BCL2 (Figure 9b), indicating that IS39 does not influence the cytotoxic mechanism of DOX in tumour cells.

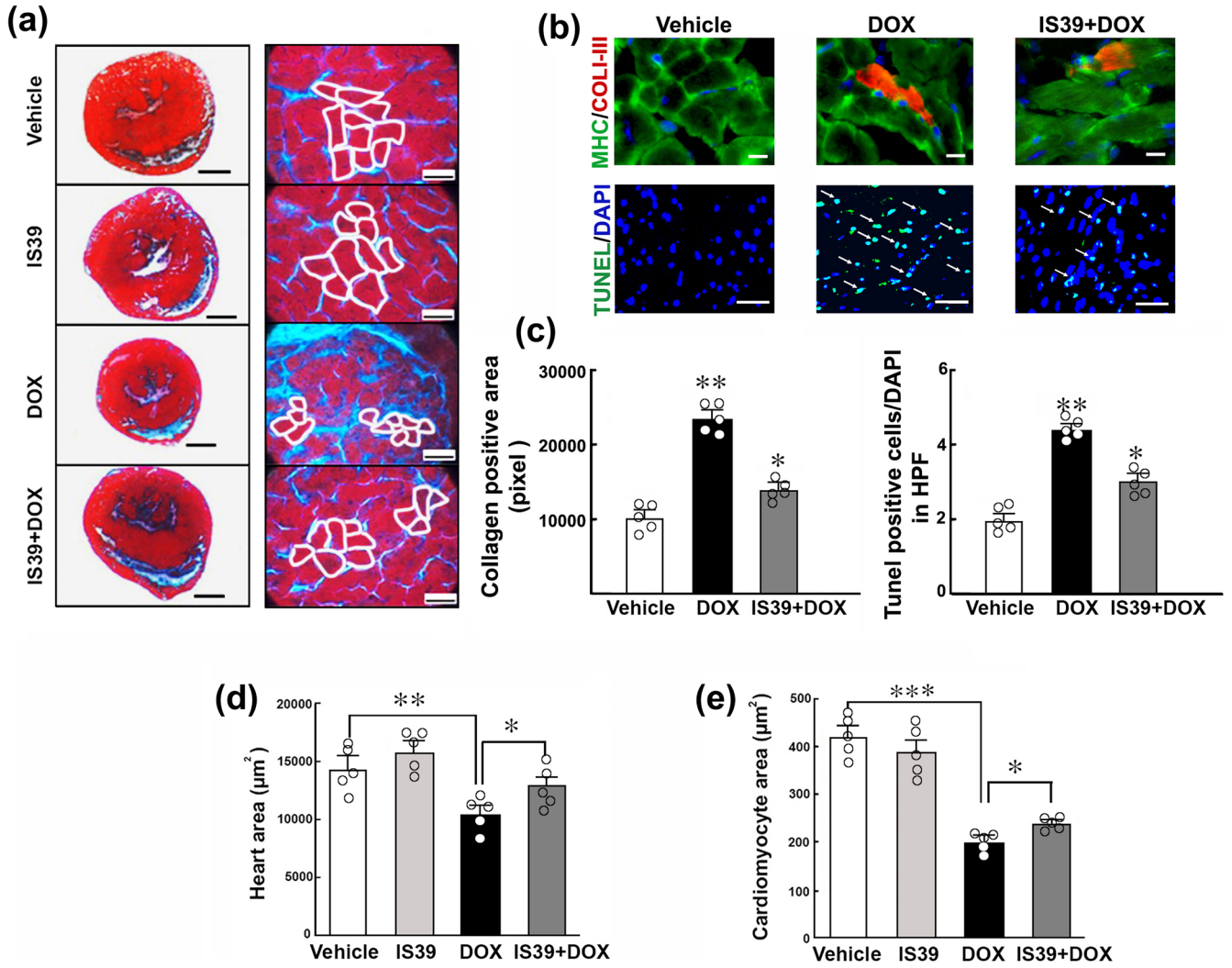

FIGURE 7 **IS39 attenuates doxorubicin (DOX)-induced cardiomyopathy and fibrosis in vivo.** (a) Representative mid-ventricular short-axis Mallory's trichrome stained heart sections, from DOX, IS39 alone, or DOX + IS39 groups (left) and corresponding high-magnification images of left ventricular (LV) myocardium illustrating cardiomyocyte borders. (right). (b) Representative LV sections stained for cardiomyocyte-specific MHC, collagen-1A (Col1A1) and TUNEL: Scale bar: 50 and 30 µm, respectively. (c) Quantification of Col1logen I and III positive area (pixels per high-power field, HPF) and TUNEL-positive nuclei (cells/HPF). (d, e) Quantification of total heart area and cardiomyocyte area (µm^2). Data are mean ± SEM, $n = 5$ animals per group; each morphometric value represents the average of ≥10 sections and ≥100 cells per images. One-way ANOVA with Bonferroni's multiple comparison test; *$P < 0.05$ versus DOX, **$P < 0.01$, ***$P < 0.001$ versus vehicle.

TABLE 4 Quantitative data for echocardiographic measurements.

Group	Heart rate (bpm)	LVESD	LVEDD	EF (%)	LVFS (%)	CO (ml min^{-1})
Vehicle ($n = 12$)	525 ± 15	2.59 ± 0.04	3.86 ± 0.03	68.0 ± 1.6	32.6 ± 0.9	51.4 ± 3.1
DOX ($n = 6$)	435 ± 15***	3.10 ± 0.03 ***	4.10 ± 0.03***	55.2 ± 1.0***	24.0 ± 0.9***	41.2 ± 1.5***
IS39 ($n = 102$)	503 ± 18 ns	2.70 ± 0.04*	3.85 ± 0.03 ns	64.0 ± 2.0 ns	30.0 ± 1.0 ns	46.2 ± 2.2 ns
DOX + IS39 ($n = 6$)	455 ± 18*†	2.65 ± 0.03†††	3.87 ± 0.04††	67.0 ± 1.5†††	31.5 ± 0.5†††	44.0 ± 2.7†

Note: SV = (LVEDD^3 − LVESD^3), CO = HR × SV. Data are presented as mean ± SEM. Statistical analysis was performed using one-way ANOVA followed by Bonferroni's multiple comparison test. $P < .05$ was considered statistically significant. Cardiac Functional Parameters (mean ± SEM).
Abbreviations: CO, cardiac output; EF, ejection fraction; HR, heart rate; LVEDD, Left ventricular end diastolic diameter; LVESD, left ventricular end systolic diameter; LVFS, left ventricular fractional shortening; ns, not significant versus vehicle; SV, stroke volume.
*$p < 0.05$ compared with vehicle.
***$p < 0.001$ compared with vehicle.
†$p < .05$ compared with doxorubicin (DOX).
††$p < .01$ compared with DOX.
†††$p < .001$ compared with DOX.

TABLE 5 Heart to body weight parameters in mice groups.

Group	Body weight (g)	Heart weight (mg)	Heart/body weight (%)
Vehicle ($n = 12$)	25.2 ± 0.8	112.6 ± 3.0	0.46 ± 0.01
IS39 ($n = 10$)	24.9 ± 1.1 ns	112.9 ± 2.0 ns	0.43 ± 0.01 ns
DOX ($n = 6$)	20.8 ± 1.0**	84.0 ± 1.4***	0.40 ± 0.01**
IS39 + DOX ($n = 6$)	18.8 ± 1.0**†	87.0 ± 1.0††	0.46 ± 0.01†††

Note: Statistical analysis was performed using one-way ANOVA followed by Bonferroni's multiple comparison test. Heart weight/body weight parameters (mean ± SEM).
*$p < .05$ versus vehicle.
**$p < .01$ versus vehicle.
***$P < .001$ versus vehicle.
†$p < .05$ versus doxorubicin (DOX).
††$P < .01$ versus DOX.
†††$P < .001$ versus DOX.

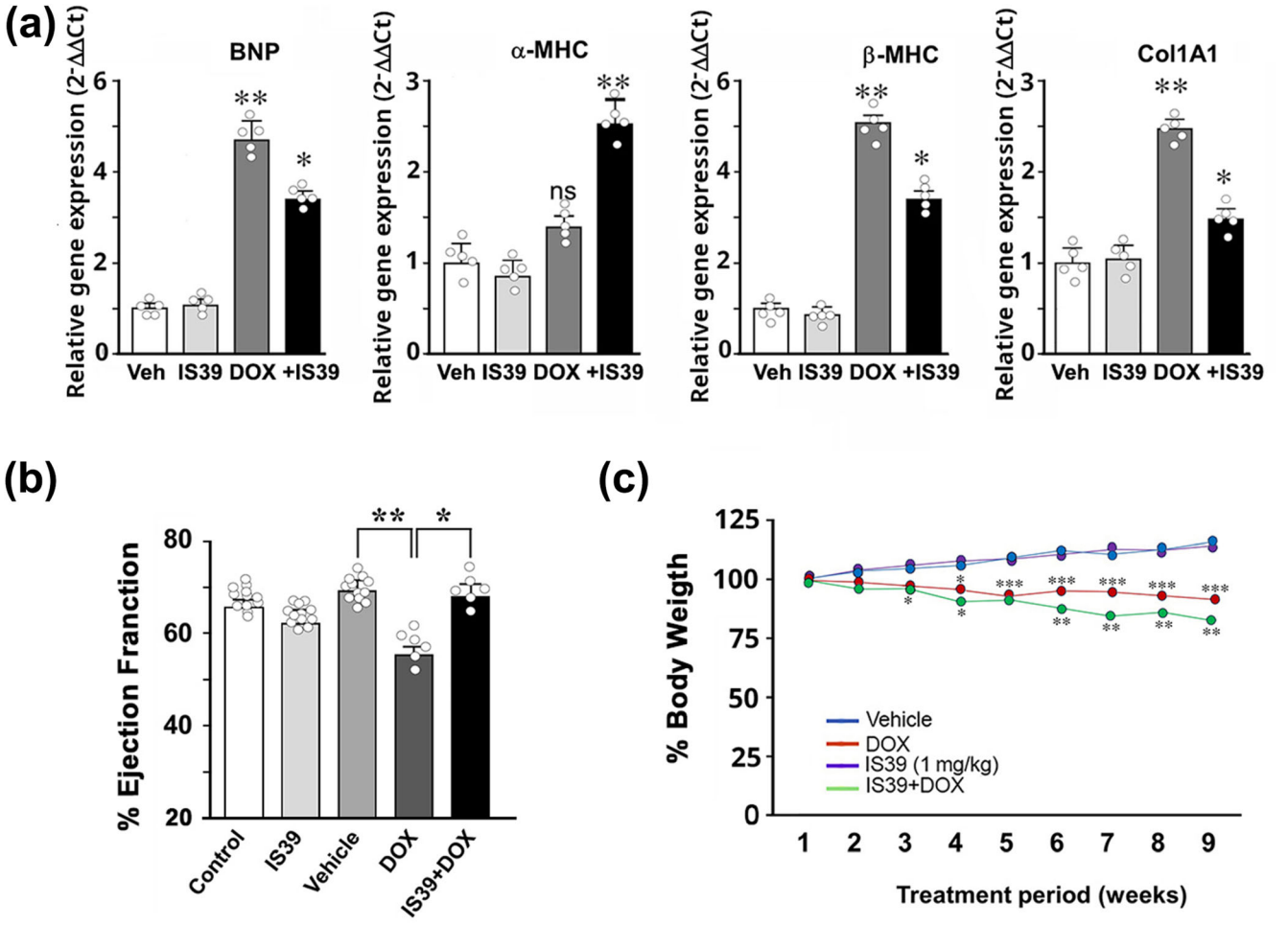

FIGURE 8 **IS39 modulates doxorubicin (DOX)-induced changes in cardiac gene expression and function.** (a) RT–PCR analysis of fibrosis-related and cardiomyopathy marker genes in mouse hearts. mRNA levels were quantified by the $2^{-}\Delta\Delta Ct$ method after normalisation to GAPDH and β-actin and are expressed as fold change relative to the vehicle group (mean ± SEM, $n = 5$ hearts per group; each sample measured in technical triplicate). One-way ANOVA with Bonferroni's test; *$P < .05$ versus DOX, **$P < .01$ versus vehicle. (b) Left ventricular ejection fraction (%) assessed by transthoracic echocardiography. Data are mean ± SEM ($n = 10$ for control, IS39 and Vehicle groups, $n = 5$ for DOX and IS39+DOX). Data were analysed by one-way ANOVA followed by Bonferroni's multiple comparison test: **$P < 0.05$ versus vehicle treated group. *$P < 0.05$ versus DOX-treated group. (c) Body-weight changes during treatment, expressed as percent of baseline. Data in Figure 8b,c are mean ± SEM, $n = 5$ animals per group. One-way ANOVA with Bonferroni's test; *$P < 0.05$ versus DOX, **$P < 0.01$ versus vehicle.

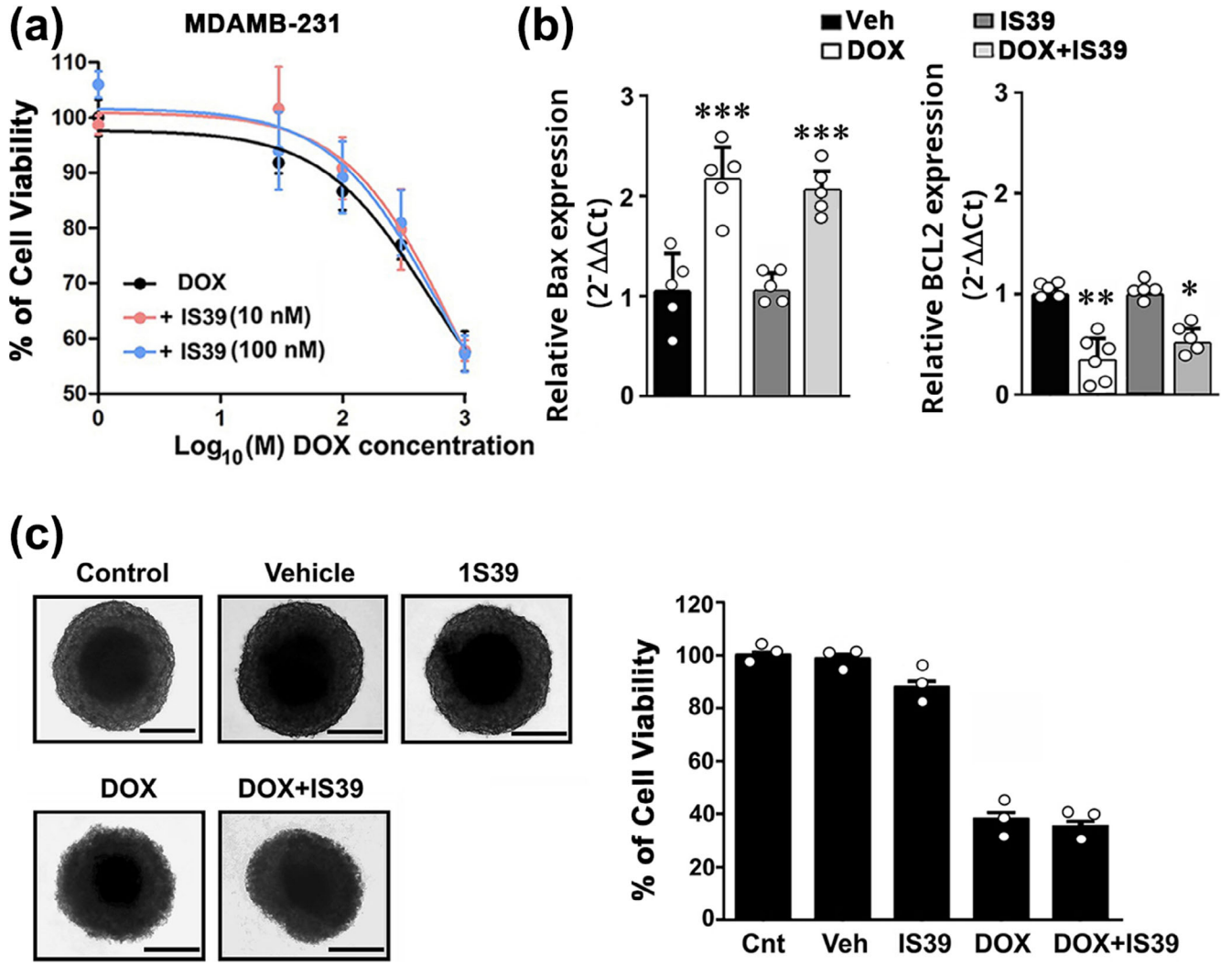

FIGURE 9 **IS39 does not interfere doxorubicin (DOX)-mediated cytotoxicity in breast cancer 2D and 3D models.** (a) Viability of MDA-MB-231 human breast cancer cells exposed to different DOX concentrations with or without IS39 (10 or 100 nM). Viability is expressed as percent of vehicle (mean ± SEM, $n = 5$ independent experiments, each in triplicate). One-way ANOVA with Bonferroni's test; $^{*}P < 0.05$, $^{**}P < 0.01$, $^{***}P < 0.001$ versus vehicle. (b) RT-qPCR analysis of BCL2 and BAX mRNA in MDA-MB-231 cells treated with vehicle, DOX, IS39 or DOX + IS39. mRNA levels were quantified by the $2^{-}\Delta\Delta$Ct method after normalisation to GAPDH and β-actin and are expressed as fold change relative to vehicle (mean ± SEM, $n = 5$ independent experiments, each in technical duplicate). One-way ANOVA with Bonferroni's test; $^{*}P < 0.05$ versus control and IS39, $^{**}P < 0.01$ versus control, $^{***}P < 0.001$ versus vehicle or IS39. (c) Effect of DOX (3 μM) ± IS39 (100 nM) on viability of human 3D breast cancer spheroids composed of MDA-MB-231, human HUVEC endothelial cells and fibroblasts. Viability is expressed as percent of untreated control (mean ± SEM, $n = 3$ independent experiments, 10 spheroids per group/condition). Each dot represents the mean of technical replicates. DOX alone and in the present of IS39 reduced spheroid viability by >60% compared to vehicle treated or control spheroids. As n=3 for these experiments, statistical analysis was not carried out, and results should be regarded as preliminary.

To further assess this interaction, we employed a tumour model that more closely mimics the in vivo environment, using 3D breast cancer spheroids composed of fibroblasts, endothelial cells and breast cancer cells as previously described (Vincenzi et al., 2025). Treatment with DOX (3 μM) significantly reduced spheroid viability by 30.7%, and co-treatment with IS39 (30 nM) did not significantly modify this effect (33.4%; Figure 9c).

Overall, these 2D and 3D data demonstrate that IS39 does not compromise the anticancer activity of DOX, supporting its safety and compatibility in cancer therapeutic contexts.

4 | DISCUSSION

4.1 | Advancing PKR_1 agonist development

Since the introduction of first non-peptide PKR_1 agonist, IS20 (Gasser et al., 2015) progress in refining PKR_1-targeted pharmacological agents has been limited. Our study extends this field by demonstrating that replacement of the original dehydroamide motif with a D-aminoacyl scaffold yields a new agonist, IS39, with enhanced improved systemic bioavailability, and cytoprotective, anti-fibrotic,

and antioxidant properties. These findings position IS39 as a promising lead molecule for developing selective PKR_1-directed cardioprotective therapeutics.

4.2 | Mechanistic insights and in vivo functional effects

Our data show that IS39 selectively activates PKR_1-dependent signalling in cardiomyocytes, resulting in reduced ROS production, suppression of apoptosis, and modulation of PI3K/Akt activity, that are known to support myocardial survival in DOX-treated hearts. These molecular effects translated into preserved cardiac morphology and systolic function in vivo, alongside repression of cardiomyopathy associated gene programmes. IS39 also reduced the expression of collagen-encoding genes, reinforcing its direct anti-fibrotic action. Together, these findings support a model in which PKR_1 activation mitigates maladaptive cardiac remodelling under chemotherapeutic stress.

Prior work with IS20 established that PKR_1 activation preserves endothelial integrity (Guilini et al., 2010), stimulates angiogenesis in ischaemic territories and limits doxorubicin-induced vascular injury without compromising anti-tumour efficacity (Gasser et al., 2019). The present data with IS39 are consistent with this profile, as IS39 failed to promote tumour growth in both conventional 2D cultures and 3D tumour spheroid models, indicating that PKR_1 stimulation can stabilise the endothelial barrier and repair damaged vasculature without fuelling pathological tumour angiogenesis. Collectively, these findings support a mechanistic model in which selective PKR_1 agonism favours vascular normalisation and endothelial protection, thereby reinforcing the concept of PKR_1-targeted agents as dual myocardial and vascular cardioprotective therapeutics in the cardio-oncology setting.

4.3 | Systemic and context-dependent effects of IS39

Despite the favourable cardiac phenotype, systemic IS39 treatment produced modest weight loss and did not improve overall survival in doxorubicin-treated mice, highlighting a potential liability of chronic PKR_1 activation under conditions of metabolic stress. This context-dependent effect reflects the pleiotropic nature of GPCR signalling. **Prokineticin-2**, the endogenous ligand of PKR_1, acts on hypothalamic centres that regulate appetite and energy balance and is now recognised as an appetite-regulating hormone. (Gardiner et al., 2010; Mortreux et al., 2019). Activation of central PKR_1 in this context suppresses food intake in mice under the high fat diet, whereas adipocyte-specific PKR_1 knockout mice display adiposity (Szatkowski et al., 2013; Von Hunolstein & Nebigil, 2015), supporting a role for peripheral PKR_1 signalling in limiting fat accumulation. In our study, IS39 did not further reduce food intake or body weight in lean control mice, but it did enhance body-weight loss selectively in doxorubicin-treated mice, suggesting that IS39 may unmask PKR_1-dependent anorexigenic and/or anti-adipogenic effects in a pathological, catabolic context. In addition, the energetic cost of myocardial repair driven by PKR_1-dependent Akt and ERK activation could further unmask vulnerabilities in whole-body energy homeostasis during anthracycline treatment. These context-dependent systemic effects underscore the need to delineate tissue-specific PKR_1 actions.

Ongoing work in our group includes analysis of circulating appetite-regulating hormones (including prokineticin-2) and body composition, as well as studies of IS39 in obesity- and diabetes-associated cardiomyopathy models, to better define its central and peripheral metabolic effects and to delineate its potential use in metabolic cardiomyopathy.

4.4 | Broader therapeutic implications

The combination of cardioprotective, anti-oxidant, anti-fibrotic and weight-lowering properties suggests that IS39, or peripherally restricted analogues, might be particularly relevant for obesity-associated cardiomyopathy, a setting characterised by diastolic dysfunction, myocardial fibrosis and metabolic derangement (Alpert, 2016; Packer, 2025). PKR_1's established involvement in both cardiovascular protection and energy balance raises the possibility of a 'single-target, dual-system' pharmacology analogous to **GLP-1 receptor** agonists, which improve glycaemic control while conferring cardioprotection in high-risk patients (Nauck et al., 2021; Sattar et al., 2021). Ongoing evaluation of IS39 in obesity- and diabetes-associated cardiomyopathy models will be critical to delineate central versus peripheral mechanisms, define a therapeutic window and inform the design of dose-optimised or peripherally restricted derivatives.

4.5 | Positioning among GPCR-targeted cardioprotective drugs

Conventional GPCR-directed therapies, such as β-adrenoceptor antagonists, angiotensin **AT_1 receptor** blockers and **sphingosine-1-phosphate receptor** modulators, predominantly act by chronic neurohormonal blockade or immunomodulation (Audebrand et al., 2019; Biswal et al., 2025). In contrast, IS39 exemplifies a ligand-biased approach that activates a pro-survival, pro-repair PKR_1 signalling profile, promoting endothelial and cardiomyocyte resilience without detectable loss of doxorubicin cytotoxicity in breast cancer models (Table 2). The absence of tumour growth promotion in both 2D and 3D spheroid models, together with previous data showing preserved anti-tumour efficacy during PKR_1 agonist treatment, addresses a major translational barrier for pro-angiogenic GPCR agonists in oncology.

4.6 | Implications for drug development

Our findings emphasise the need for medicinal chemistry strategies that enhance tissue specificity and minimise systemic metabolic

effects. Approaches such as peripherally restricted analogues, nanoparticle-based cardiac delivery, or ligand optimisation guided by structure–activity relationships may improve translational readiness. IS39 provides a tractable scaffold for such efforts and a mechanistic foundation for developing next-generation PKR_1 agonists with favourable pharmacokinetic and safety profiles.

5 | STUDY LIMITATION

This study has limitations. IS39 induced weight loss and failed to improve survival in DOX-treated mice, suggesting off-target or centrally mediated metabolic effects. Although IS39 selectively activated PKR_1 in cardiomyocytes, broader GPCR crosstalk or off-target activity cannot be excluded. Only male mice were studied, and sex-specific differences in DOX cardiotoxicity remain unexamined. Long-term and chronic dosing regimens were not assessed, and the delivery route used may not represent optimal clinical translation. These limitations underscore the need for future studies addressing pharmacokinetics, receptor specificity and tissue-targeted delivery.

6 | CONCLUSION

IS39 is a novel PKR_1 agonist that provides robust protection against DOX-induced cardiac injury by engaging antioxidant, anti-fibrotic and pro-survival pathways. Although systemic metabolic effects currently limit translational applicability, IS39 establishes a strong pharmacological basis for PKR_1-targeted cardioprotection. Future optimisation aimed at enhancing cardiac selectivity and reducing catabolic side effects may yield clinically viable therapeutics for cardio–oncology and metabolic cardiomyopathies.

AUTHOR CONTRIBUTIONS

Anais Audebrand: Investigation; methodology. **Simone Brogi:** Conceptualization; investigation; methodology. **Mustafa Tezeren:** Conceptualization; investigation; methodology. **Andrea Tafi:** Conceptualization; investigation; methodology. **Omer H. Ocak:** Conceptualization; funding acquisition; validation; project administration. **Hasan Koyuncu:** Conceptualization; funding acquisition; validation; project administration. **Igor Tetko:** Conceptualization; investigation; funding acquisition; project administration; validation; writing—review and editing. **Laurent Désaubry:** Conceptualization; writing—original draft; methodology; validation; writing—review and editing; funding acquisition; supervision. **Canan G. Nebigil:** Conceptualization; funding acquisition; writing—original draft; methodology; validation; visualization; writing—review and editing; project administration; supervision.

ACKNOWLEDGEMENTS

This study was supported by grants Fondation de France and European Research Area Network on Cardiovascular diseases (ERA-CVD) 'cardiooncology' grant and Agence Nationale de la Recherche grants (ANR0005). A.A. and M.T. were supported by ANR0005. We thank IGBMC, Illkirch, for providing cancer cell lines. Open access publication funding provided by COUPERIN CY26.

CONFLICT OF INTEREST STATEMENT

The authors declare that they have no known competing financial interests or personal relationships that could have appeared to influence the work reported in this paper.

DATA AVAILABILITY STATEMENT

The data that support the findings of this study are available from the corresponding author upon reasonable request.

DECLARATION OF TRANSPARENCY AND SCIENTIFIC RIGOUR

This Declaration acknowledges that this paper adheres to the principles for transparent reporting and scientific rigour of preclinical research as stated in the *BJP* guidelines for Design and Analysis, Immunoblotting and Immunohistochemistry, and Animal Experimentation and as recommended by funding agencies, publishers and other organisations engaged with supporting research.

ORCID

Simone Brogi https://orcid.org/0000-0001-9375-6242

REFERENCES

Alexander, S. P. H., Cidlowski, J. A., Gibb, A. J., Kelly, E., Mathie, A. A., Peach, C. J., Veale, E. L., Armstrong, J. F., Faccenda, E., Harding, S. D., Southan, C., Davies, J. A., Coons, L., Fuller, P. J., Korach, K. S., McDonell, D. P., Oakley, R., Radi, S., Safi, R., … Young, M. J. (2025). The Concise Guide to PHARMACOLOGY 2025/26: Nuclear hormone receptors. *British Journal of Pharmacology*, *182*(Suppl 1), S242–S258. https://doi.org/10.1111/bph.70232

Alexander, S. P. H., Fabbro, D., Gibb, A. J., Kelly, E., Mathie, A. A., Peach, C. J., Veale, E. L., Armstrong, J. F., Faccenda, E., Harding, S. D., Southan, C., Davies, J. A., Annett, S., Boison, D., Burns, K. E., Dessauer, C., Gertsch, J., Helsby, N. A., Izzo, A. A., … Wong, S. S. (2025). The Concise Guide to PHARMACOLOGY 2025/26: Enzymes. *British Journal of Pharmacology*, *182*(Suppl 1), S307–S403. https://doi.org/10.1111/bph.70234

Alexander, S. P. H., Roberts, R. E., Broughton, B. R. S., Sobey, C. G., George, C. H., Stanford, S. C., Cirino, G., Docherty, J. R., Giembycz, M. A., Hoyer, D., Insel, P. A., Izzo, A. A., Ji, Y., MacEwan, D. J., Mangum, J., Wonnacott, S., & Ahluwalia, A. (2018). Goals and practicalities of immunoblotting and immunohistochemistry: A guide for submission to the British Journal of Pharmacology. *British Journal of Pharmacology*, *175*, 407–411. https://doi.org/10.1111/bph.14112

Alexander, W., Al-hosaini, K., Bäck, M., Baker, J. G., Barnes, N. M., Bathgate, R., Beaulieu, J.-M., Beck-Sickinger, A. G., Behrens, M., Bennett, K. A., Bernstein, K. E., Bettler, B., Birdsall, N. J. M., Blaho, V. A., Bonaventure, P., Boulay, F., Bousquet, C., Bräuner-Osborne, H., Brown, A. J., … Zaidman, N. (2025). The Concise Guide to PHARMACOLOGY 2025/26: G protein-coupled receptors. *British Journal of Pharmacology*, *182*(Suppl 1), S24–S151. https://doi.org/10.1111/bph.70230

Alpert, M. A. (2016). Severe obesity and acute decompensated heart failure: New insights into prevalence and prognosis. *JACC: Heart Failure*, *4*(12), 932–934. https://doi.org/10.1016/j.jchf.2016.10.008

Armenian, S. H., Lacchetti, C., Barac, A., Carver, J., Constine, L. S., Denduluri, N., Dent, S., Douglas, P. S., Durand, J.-B., Ewer, M., Fabian, C., Hudson, M., Jessup, M., Jones, L. W., Ky, B., Mayer, E. L., Moslehi, J., Oeffinger, K., Ray, K., … Lenihan, D. (2017). Prevention and monitoring of cardiac dysfunction in survivors of adult cancers: American Society of Clinical Oncology clinical practice guideline. *Journal of Clinical Oncology*, *35*(8), 893–911. https://doi.org/10.1200/JCO.2016.70.5400

Arora, H., Vincenzi, M., Audebrand, A., Kremic, A., Gentile, C., Désaubry, L., & Nebigil, C. G. (2025). MiR-124 orchestrates epicardial-mesenchymal-transformation and paracrine cardiomyocyte maturation in epicardial-specific tcf21-PKR1 knockout mice. *Stem Cells*. https://doi.org/10.1093/stmcls/sxaf082

Audebrand, A., Desaubry, L., & Nebigil, C. G. (2019). Targeting GPCRs against cardiotoxicity induced by anticancer treatments. *Frontiers in Cardiovascular Medicine*, *6*, 194. https://doi.org/10.3389/fcvm.2019.00194

Biswal, N., Harish, R., Roshan, M., Samudrala, S., Jiao, X., Pestell, R. G., & Ashton, A. W. (2025). Role of GPCR signaling in anthracycline-induced cardiotoxicity. *Cells*, *14*(3), 169. https://doi.org/10.3390/cells14030169

Bouleftour, W., Mery, B., Rowinski, E., Rivier, C., Daguenet, E., & Magne, N. (2021). Cardio-oncology preclinical models: A comprehensive review. *Anticancer Research*, *41*(11), 5355–5364. https://doi.org/10.21873/anticanres.15348

Cardinale, D., Colombo, A., Bacchiani, G., Tedeschi, I., Meroni, C. A., Veglia, F., Civelli, M., Lamantia, G., Colombo, N., Curigliano, G., Fiorentini, C., & Cipolla, C. M. (2015). Early detection of anthracycline cardiotoxicity and improvement with heart failure therapy. *Circulation*, *131*(22), 1981–1988. https://doi.org/10.1161/CIRCULATIONAHA.114.013777

Curtis, M. J., Alexander, S. P. H., Cortese-Krott, M., Kendall, D. A., Martemyanov, K. A., Mauro, C., Panettieri, R. A. Jr., Papapetropoulos, A., Patel, H. H., Santo, E. E., Schulz, R., Stefanska, B., Stephens, G. J., Teixeira, M. M., Vergnolle, N., Wang, X., & Ferdinandy, P. (2025 Apr). Guidance on the planning and reporting of experimental design and analysis. *British Journal of Pharmacology*, *182*(7), 1413–1415. https://doi.org/10.1111/bph.17441

Dormishian, M., Turkeri, G., Urayama, K., Nguyen, T. L., Boulberdaa, M., Messaddeq, N., Renault, G., Henrion, D., & Nebigil, C. G. (2013). Prokineticin receptor-1 is a new regulator of endothelial insulin uptake and capillary formation to control insulin sensitivity and cardiovascular and kidney functions. *Journal of the American Heart Association*, *2*(5), e000411. https://doi.org/10.1161/JAHA.113.000411

Gardiner, J. V., Bataveljic, A., Patel, N. A., Bewick, G. A., Roy, D., Campbell, D., Greenwood, H. C., Murphy, K. G., Hameed, S., Jethwa, P. H., Ebling, F. J., Vickers, S. P., Cheetham, S., Ghatei, M. A., Bloom, S. R., & Dhillo, W. S. (2010). Prokineticin 2 is a hypothalamic neuropeptide that potently inhibits food intake. *Diabetes*, *59*(2), 397–406. https://doi.org/10.2337/db09-1198

Gasser, A., Brogi, S., Urayama, K., Nishi, T., Kurose, H., Tafi, A., Ribeiro, N., Désaubry, L., & Nebigil, C. G. (2015). Discovery and cardioprotective effects of the first non-peptide agonists of the G protein-coupled prokineticin receptor-1. *PLoS One*, *10*(4), e0121027. https://doi.org/10.1371/journal.pone.0121027

Gasser, A., Chen, Y. W., Audebrand, A., Daglayan, A., Charavin, M., Escoubet, B., Karpov, P., Tetko, I., Chan, M. W. Y., Cardinale, D., Désaubry, L., & Nebigil, C. G. (2019). Prokineticin receptor-1 signaling inhibits dose- and time-dependent anthracycline-induced cardiovascular toxicity via myocardial and vascular protection. *JACC CardioOncology*, *1*(1), 84–102. https://doi.org/10.1016/j.jaccao.2019.06.003

Guilini, C., Urayama, K., Turkeri, G., Dedeoglu, D. B., Kurose, H., Messaddeq, N., & Nebigil, C. G. (2010). Divergent roles of prokineticin receptors in the endothelial cells: Angiogenesis and fenestration. *American Journal of Physiology. Heart and Circulatory Physiology*, *298*(3), H844–H852. https://doi.org/10.1152/ajpheart.00898.2009

Han, Z., Xia, Z., Xia, J., Tetko, I. V., & Wu, S. (2025). The state-of-the-art machine learning model for plasma protein binding prediction: Computational modeling with OCHEM and experimental validation. *European Journal of Pharmaceutical Sciences*, *204*, 106946. https://doi.org/10.1016/j.ejps.2024.106946

Hsu, P. Y., Mammadova, A., Benkirane-Jessel, N., Desaubry, L., & Nebigil, C. G. (2021). Updates on anticancer therapy-mediated vascular toxicity and new horizons in therapeutic strategies. *Frontiers in Cardiovascular Medicine*, *8*, 694711. https://doi.org/10.3389/fcvm.2021.694711

Lilley, E., Stanford, S. C., Kendall, D. E., Alexander, S. P. H., Cirino, G., Docherty, J. R., George, C. H., Insel, P. A., Izzo, A. A., Ji, Y., Panettieri, R. A., Sobey, C. G., Stefanska, B., Stephens, G., Teixeira, M., & Ahluwalia, A. (2020). ARRIVE 2.0 and the *British Journal of Pharmacology*: Updated guidance for 2020. *British Journal of Pharmacology*, *177*(16), 3611. https://doi.org/10.1111/bph.15178

Linders, A. N., Dias, I. B., Lopez Fernandez, T., Tocchetti, C. G., Bomer, N., & Van der Meer, P. (2024). A review of the pathophysiological mechanisms of doxorubicin-induced cardiotoxicity and aging. *NPJ Aging*, *10*(1), 9. https://doi.org/10.1038/s41514-024-00135-7

Lyon, A. R., Dent, S., Stanway, S., Earl, H., Brezden-Masley, C., Cohen-Solal, A., Tocchetti, C. G., Moslehi, J. J., Groarke, J. D., Bergler-Klein, J., Khoo, V., Tan, L. L., Anker, M. S., von Haehling, S., Maack, C., Pudil, R., Barac, A., Thavendiranathan, P., Ky, B., … Lenihan, D. (2020). Baseline cardiovascular risk assessment in cancer patients scheduled to receive cardiotoxic cancer therapies: A position statement and new risk assessment tools from the cardio-oncology study group of the heart failure Association of the European Society of Cardiology in collaboration with the International Cardio-Oncology Society. *European Journal of Heart Failure*, *22*(11), 1945–1960. https://doi.org/10.1002/ejhf.1920

Maddox, T. M., Januzzi, J. L. Jr., Allen, L. A., Breathett, K., Brouse, S., Butler, J., Davis, L. L., Fonarow, G. C., Ibrahim, N. E., Lindenfeld, J., Masoudi, F. A., Motiwala, S. R., Oliveros, E., Walsh, M. N., Wasserman, A., Yancy, C. W., & Youmans, Q. R. (2024). 2024 ACC expert consensus decision pathway for treatment of heart failure with reduced ejection fraction: A report of the American College of Cardiology solution set oversight committee. *Journal of the American College of Cardiology*, *83*(15), 1444–1488. https://doi.org/10.1016/j.jacc.2023.12.024

Mortreux, M., Foppen, E., Denis, R. G., Montaner, M., Kassis, N., Denom, J., Vincent, M., Fumeron, F., Kujawski-Lafourcade, M., Andréelli, F., Balkau, B., Marre, M., Roussel, R., Magnan, C., Gurden, H., & Migrenne-Li, S. (2019). New roles for prokineticin 2 in feeding behavior, insulin resistance and type 2 diabetes: Studies in mice and humans. *Molecular Metabolism*, *29*, 182–196. https://doi.org/10.1016/j.molmet.2019.08.016

Nauck, M. A., Quast, D. R., Wefers, J., & Pfeiffer, A. F. H. (2021). The evolving story of incretins (GIP and GLP-1) in metabolic and cardiovascular disease: A pathophysiological update. *Diabetes, Obesity & Metabolism*, *23*(Suppl 3), 5–29. https://doi.org/10.1111/dom.14496

Nebigil, C. G. (2017). Prokineticin is a new linker between obesity and cardiovascular diseases. *Frontiers in Cardiovascular Medicine*, *4*, 20. https://doi.org/10.3389/fcvm.2017.00020

Nebigil, C. G., Chan, M. W. Y., & Rassaf, T. (2020). Editorial: Emerging challenges of cardiovascular and metabolic dysfunctions in cardio-oncology: From bench to bedside. *Frontiers in Cardiovascular Medicine*, *7*, 148. https://doi.org/10.3389/fcvm.2020.00148

Nebigil, C. G., & Desaubry, L. (2018). Updates in anthracycline-mediated cardiotoxicity. *Frontiers in Pharmacology*, *9*, 1262. https://doi.org/10.3389/fphar.2018.01262

Nguyen, T. L., Gasser, A., & Nebigil, C. G. (2013). Role of prokineticin receptor-1 in epicardial progenitor cells. *Journal of Developmental Biology*, *1*(1), 20–31. https://doi.org/10.3390/jdb1010020

Packer, M. (2025). The adipokine hypothesis of heart failure with a preserved ejection fraction: A novel framework to explain pathogenesis

and guide treatment. *Journal of the American College of Cardiology*, *86*(16), 1269–1373. https://doi.org/10.1016/j.jacc.2025.06.055

Percie du Sert, N., Hurst, V., Ahluwalia, A., Alam, S., Avey, M. T., Baker, M., Browne, W. J., Clark, A., Cuthill, I. C., Dirnagl, U., Emerson, M., Garner, P., Holgate, S. T., Howells, D. W., Karp, N. A., Lazic, S. E., Lidster, K., MacCallum, C. J., Macleod, M., … Würbel, H. (2020). The ARRIVE guidelines 2.0: Updated guidelines for reporting animal research. *PLoS Biology*, *18*(7), e3000410. https://doi.org/10.1371/journal.pbio.3000410

Qureshi, R., Kindo, M., Boulberdaa, M., von Hunolstein, J. J., Steenman, M., & Nebigil, C. G. (2018). A prokineticin-driven epigenetic switch regulates human epicardial cell stemness and fate. *Stem Cells*, *36*(10), 1589–1602. https://doi.org/10.1002/stem.2866

Sattar, N., Lee, M. M. Y., Kristensen, S. L., Branch, K. R. H., Del Prato, S., Khurmi, N. S., Lam, C. S. P., Lopes, R. D., McMurray, J. J. V., Pratley, R. E., Rosenstock, J., & Gerstein, H. C. (2021). Cardiovascular, mortality, and kidney outcomes with GLP-1 receptor agonists in patients with type 2 diabetes: A systematic review and meta-analysis of randomised trials. *The Lancet Diabetes & Endocrinology*, *9*(10), 653–662. https://doi.org/10.1016/S2213-8587(21)00203-5

Sosnin, S., Karlov, D., Tetko, I. V., & Fedorov, M. V. (2019). Comparative study of multitask toxicity modeling on a broad chemical space. *Journal of Chemical Information and Modeling*, *59*(3), 1062–1072. https://doi.org/10.1021/acs.jcim.8b00685

Szatkowski, C., Vallet, J., Dormishian, M., Messaddeq, N., Valet, P., Boulberdaa, M., Metzger, D., Chambon, P., & Nebigil, C. G. (2013). Prokineticin receptor 1 as a novel suppressor of preadipocyte proliferation and differentiation to control obesity. *PLoS One*, *8*(12), e81175. https://doi.org/10.1371/journal.pone.0081175

Tetko, I. V., Tanchuk, V. Y., Kasheva, T. N., & Villa, A. E. (2001). Estimation of aqueous solubility of chemical compounds using E-state indices. *Journal of Chemical Information and Computer Sciences*, *41*(6), 1488–1493. https://doi.org/10.1021/ci000392t

Urayama, K., Guilini, C., Messaddeq, N., Hu, K., Steenman, M., Kurose, H., Ert, G., & Nebigil, C. G. (2007). The prokineticin receptor-1 (GPR73) promotes cardiomyocyte survival and angiogenesis. *The FASEB Journal*, *21*(11), 2980–2993. https://doi.org/10.1096/fj.07-8116com

Urayama, K., Guilini, C., Turkeri, G., Takir, S., Kurose, H., Messaddeq, N., Dierich, A., & Nebigil, C. G. (2008). Prokineticin receptor-1 induces neovascularization and epicardial-derived progenitor cell differentiation. *Arteriosclerosis, Thrombosis, and Vascular Biology*, *28*(5), 841–849. https://doi.org/10.1161/ATVBAHA.108.162404

Valceski, M., Engels, E., Vogel, S., Paino, J., Potter, D., Hollis, C., … Tehei, M. (2024). A novel approach to double-strand DNA break analysis through gamma-H2AX confocal image quantification and biodosimetry. *Scientific Reports*, *14*(1), 27591. https://doi.org/10.1038/s41598-024-76683-5

Vincenzi, M., Kremic, A., Jouve, A., Lattanzi, R., Miele, R., Benharouga, M., … Nebigil, C. G. (2023). Therapeutic potential of targeting prokineticin receptors in diseases. *Pharmacological Reviews*, *75*(6), 1167–1199. https://doi.org/10.1124/pharmrev.122.000801

Vincenzi, M., Kremic, A., Tscheiller, N. N., Hsu, P. Y., Chan, M. W. Y., Lattanzi, R., & Nebigil, C. G. (2025). Identification of prokineticin-2 as potential pharmacodynamic biomarker for overcoming doxorubicin resistance in multicellular breast cancer spheroids. *British Journal of Pharmacology*, *183*, 491–504. https://doi.org/10.1111/bph.70204

Vincenzi, M., & Nebigil, C. G. (2025). Uncovering the role of prokineticin pathway on epicardial adipose tissue (EAT) development and EAT-associated cardiomyopathy. *Trends in Cardiovascular Medicine*, *35*, 328–338. https://doi.org/10.1016/j.tcm.2025.02.006

Von Hunolstein, J.-J., & Nebigil, C. G. (2015). Can prokineticin prevent obesity and insulin resistance? *Current Opinion in Endocrinology, Diabetes and Obesity*, *22*(5), 367–373. https://doi.org/10.1097/MED.0000000000000185

Wang, J., Gareri, C., & Rockman, H. A. (2018). G-protein-coupled receptors in heart disease. *Circulation Research*, *123*(6), 716–735. https://doi.org/10.1161/CIRCRESAHA.118.311403

Yakavets, I., Francois, A., Benoit, A., Merlin, J. L., Bezdetnaya, L., & Vogin, G. (2020). Advanced co-culture 3D breast cancer model for investigation of fibrosis induced by external stimuli: optimization study. *Scientific Reports*, *10*(1), 21273. https://doi.org/10.1038/s41598-020-78087-7

Yu, Y., Dai, M., Xu, W., Chen, S., & Lu, Q. (2021). Close to real: Large-volume 3D cell spheroids on a superamphiphobic surface. *Advanced Materials Interfaces*, *8*(9), 2100039. https://doi.org/10.1002/admi.202100039

Zamorano, J. L., Lancellotti, P., Munoz, D. R., Aboyans, V., Asteggiano, R., Galderisi, M., Habib, G., Lenihan, D. J., Lip, G. Y. H., Lyon, A. R., Fernandez, T. L., Mohty, D., Piepoli, M. F., Tamargo, J., Torbicki, A., & Suter, T. M. (2016). 2016 ESC position paper on cancer treatments and cardiovascular toxicity developed under the auspices of the ESC Committee for Practice Guidelines. *Kardiologia Polska*, *74*(11), 1193–1233. https://doi.org/10.5603/KP.2016.0156

SUPPORTING INFORMATION

Additional supporting information can be found online in the Supporting Information section at the end of this article.

How to cite this article: Audebrand, A., Brogi, S., Tezeren, M., Tafi, A., Ocak, O. H., Koyuncu, H., Tetko, I., Désaubry, L., & Nebigil, C. G. (2026). Second-generation prokineticin PKR_1 receptor agonists: Advancing cardioprotection against chemotherapy-induced toxicity. *British Journal of Pharmacology*, 1–18. https://doi.org/10.1111/bph.70394